# SRC activation skews cell fate from apoptosis to senescence

**Carlos Anerillas**
National Institutes of Health https://orcid.org/0000-0003-4424-7913
**Allison Herman**
National Institutes of Health
**Martina Rossi**
National Institutes of Health
**Rachel Munk**
National Institutes of Health
**Elin Lehrmann**
National Institutes of Health https://orcid.org/0000-0002-9869-9475
**Jennifer Martindale**
National Institutes of Health
**Chang-Yi Cui**
National Institutes of Health
**Kotb Abdelmohsen**
National Institutes of Health
**Supriyo De**
National Institutes of Health
**Myriam Gorospe** ( myriam-gorospe@nih.gov )
Nat Inst on Aging, NIH

**Article**

**Keywords:** DNA damage, apoptosis, senescence, SRC activation

**Posted Date:** April 23rd, 2021

**DOI:** https://doi.org/10.21203/rs.3.rs-437609/v1

# SRC activation skews cell fate from apoptosis to senescence

Carlos Anerillas*, Allison B. Herman, Martina Rossi, Rachel Munk, Elin Lehrmann, Jennifer L. Martindale, Chang-Yi Cui, Kotb Abdelmohsen, Supriyo De, and Myriam Gorospe*

Laboratory of Genetics and Genomics, National Institute on Aging Intramural Research Program, National Institutes of Health, Baltimore, Maryland, USA

*Correspondence:
Laboratory of Genetics and Genomics
NIA IRP, NIH
251 Bayview Blvd.
Baltimore, MD 21224, USA
myriam-gorospe@nih.gov

Running Title: SRC promotes cell senescence

## Abstract

Cells responding to DNA damage implement complex adaptive programs that often culminate in two distinct outcomes: apoptosis or senescence. To systematically identify factors driving each response, we analyzed human IMR-90 fibroblasts exposed to increasing doses of the genotoxin etoposide and identified SRC as a key kinase contributing to this dichotomous decision. SRC was activated by low (50 μM) etoposide but not by high (200 μM) etoposide levels. With low DNA damage, SRC-mediated activation of p38 critically promoted cell survival and senescence, and increased pro-survival BCL2L2 levels, while SRC-mediated repression of p53 prevented a rise in pro-apoptotic PUMA levels. With high DNA damage, SRC was not activated, leading to elevation of p53, inhibition of p38, and apoptosis. In mice exposed to DNA damage, pharmacologic inhibition of SRC prevented tissue accumulation of senescent cells. We propose that inhibiting SRC could be exploited to induce senescent-cell apoptosis in tissues to improve health outcomes.

Senescent cells arise in tissues responding to sublethal damage to cellular components. They are characterized by morphological changes, indefinite cell cycle arrest with increased expression of cyclin-dependent kinase inhibitors p21 (CDKN1A) and p16 (CDKN2A), elevated resistance to apoptosis, and metabolic alterations including increased lysosomal function and activation of a senescence-associated β-galactosidase enzyme (SA-β-gal)[1]. They also actively secrete pro-inflammatory molecules and tissue-remodeling factors, a trait known as the senescence-associated secretory phenotype (SASP)[1]. Senescent cells are beneficial for physiological processes such as tissue repair, embryonic development, and cancer prevention; however, the accumulation of senescent cells can be detrimental to tissue function, disrupts organ homeostasis, and contributes to disease development[2]. Accordingly, the increased presence of senescent cells in aging tissues and organs has been linked to many age-associated physiologic declines and chronic diseases[3]. Recently, novel therapeutic strategies ('senotherapies') aiming to eliminate senescent cells in tissues ('senolysis') have been developed, but their precise mechanisms of action are not fully understood and their efficacy in clinical settings is still being investigated[4]. An alternative emerging strategy to reduce the senescent-cell compartment for health benefit aims to prevent the buildup of senescent cells in tissues before they become detrimental.

Although DNA-damaging stimuli can trigger apoptotic cell death, they can also be potent inducers of senescence. Whether the cell outcome is apoptosis or senescence is influenced by the cell type and the extent and nature of the genotoxic injury[5]. In this regard, senescent cells represent a state of increased resistance to apoptotic cell death, with elevated activity of pro-survival pathways such as those elicited by the BCL2 family of antiapoptotic proteins[6,7], although some pro-apoptotic effectors are also increased in senescence[8]. The specific molecular determinants of the decision between apoptosis and senescence have not been identified, but as senolytic agents generally operate by suppressing the anti-apoptotic defense of senescent cells[9], identifying damage-sensing signaling pathways that direct the cellular response towards apoptosis or senescence can uncover senescent cell vulnerabilities and help design effective senotherapies.

Given the limited knowledge of the molecular effectors that direct response pathways towards senescence or apoptosis, we sought to study systematically these two responses in the same cell type, changing only the magnitude of damage. We hypothesized that by uncovering signaling differences between cells committed to either senescence or apoptosis, we might identify critical factors tilting cells to one response or the other. In this study, we identified the kinase SRC as a key protein that was activated in human IMR-90 fibroblasts undergoing senescence in response to DNA damage, and therefore surviving the genotoxic injury. By contrast, IMR-90 cells undergoing cell death showed much less SRC activation. Signaling through SRC is aberrantly activated in many malignant cells often via upstream receptor tyrosine kinases (RTKs)[10]. SRC modulates several major signaling pathways,

including mitogen-activated protein kinases (MAPKs), phosphoinositide 3-kinase (PI3K)/protein kinase B (AKT1), signal transducers and activators of transcription (STATs), and signaling through p53 (TP53), all central to the apoptotic and senescence programs[11,12]. In the paradigm described here, SRC activation by low levels of the DNA-damaging agent etoposide caused cells to undergo senescence and survival, with reduced p53 signaling and hence lower levels of PUMA (p53-upregulated modulator of apoptosis, a transcriptional target of p53), and activated MAPK p38 signaling, leading to increased abundance of the pro-survival protein BCL2L2. By contrast, diminished SRC activity by high levels of etoposide-triggered DNA damage, led to decreased p38 function and increased p53 function, promoting apoptosis. Similarly, in tissues of mice treated with DNA damaging agents, the accumulation of senescent cells was reduced by pharmacologic inhibition of SRC. We propose that SRC inhibition might be explored for inducing apoptosis of senescent cells in aged or damaged tissues to improve health span and disease outcomes.

## Results

### Pro-survival signaling elicited by senescence-committed cells is centered on SRC

To systematically investigate the signaling pathways that govern whether cells undergo senescence or apoptosis, we first determined the thresholds of damage that triggered each cell response. We tested a range of doses of the DNA-damaging agent etoposide in proliferating human diploid IMR-90 fibroblasts, refreshing etoposide every 3 days (**Fig. 1a,b**). Cell viability was measured at different times after etoposide treatment at doses ranging from 25 to 300 μM (**Fig. 1c**). We focused on 50 and 200 μM doses of etoposide for subsequent experiments, as both doses led to similar cell survival by 48 h; thereafter, 200 μM etoposide treatment caused cell death (**Fig. 1c**). By contrast, cells treated with 50 μM etoposide maintained viability throughout the time course, allowing us to directly compare etoposide-induced senescence (50 μM) and apoptosis (200 μM) side by side.

To study if 50 μM etoposide triggered cell senescence, we measured several well-established senescence markers. First, we assessed senescence-associated β-galactosidase (SA-β-Gal) activity in IMR-90 cells that were either left untreated or treated with 50 μM etoposide for 10 days (**Fig. 1d**); as shown, 50 μM etoposide increased SA-β-Gal activity, yielding ~80% SA-β-Gal-positive cells compared to 10% SA-β-Gal-positive in the untreated group (**Fig. 1d, *right***). Second, cell proliferation analysis by measuring BrdU incorporation (Methods) showed that cells treated with 50 μM etoposide incorporated significantly less BrdU than untreated cells (**Fig. 1e**). Third, the expression levels of senescence markers *p16* and *IL6* mRNA, monitored by reverse transcription followed by quantitative PCR (RT-qPCR) analysis, were markedly elevated by 10 days of 50 μM etoposide treatment (**Fig. 1f**).

Given that by 10 days of treatment 50 μM etoposide induced senescence while 200 μM etoposide triggered cell death, we explored the signaling status of cells in each group just 48 h into the treatment, when cells were still healthy but death or senescence decisions were likely being made. Phosphoprotein array analysis was used to evaluate the phosphorylation levels of approximately 600 residues across the human kinome to identify the most significant changes (**Supplementary Fig. 1**, **Supplementary Table 1**). Based on these changes, we identified interaction pathways involving differentially phosphorylated proteins in cells committed to senescence (50 μM) and to apoptosis (200 μM) using STRING software. The highest-ranking protein identified as most differentially represented between the two conditions was the kinase SRC (**Fig. 1g**). SRC is mainly implicated in transducing signals from the plasma membrane through many phosphorylation cascades[13] and was previously described as a pro-survival kinase in cancer[14], in keeping with a potential role in the survival of etoposide-treated IMR-90 fibroblasts. Importantly, treatment of IMR-90 cells with 50 μM etoposide increased SRC phosphorylation at tyrosine (Y) 418, while 200 μM etoposide reduced this phosphorylation event, as found by phosphoarray analysis (**Fig. 1h**) and confirmed by Western blot analysis (**Fig. 1i**). Thus, SRC activity appears to be implicated in the cell fate decision to undergo senescence or apoptosis after DNA damage by etoposide.

**Genetic modulation supports SRC involvement in promoting cell survival upon DNA damage**

Finding SRC and SRC-related proteins at the decision point between senescence and apoptosis, we next asked if modulating SRC function might affect the outcome of cells responding to DNA damage. First we reduced SRC levels by silencing using SRC-directed siRNA (siSRC); siCtrl was included in control silencing groups. After confirming the efficiency of silencing SRC protein and *SRC* mRNA by Western blot and RT-qPCR analyses, respectively (**Fig. 2a**), we examined the effect of SRC silencing on senescence induced by etoposide (50 μM). Cell viability (**Figs. 2b,c**) was markedly reduced when SRC kinase was silenced in cells treated with 50 μM etoposide compared to control cells (siCtrl), where cell survival was unchanged, suggesting that SRC contributes to the survival of cells undergoing etoposide-triggered senescence. To examine if SRC silencing specifically directed senescent cells towards apoptosis, we tested the effect of ZVAD-FMK, a broad-spectrum inhibitor of caspases (the proteases that execute the apoptotic program[15]). While ZVAD-FMK had no effect on the viability of cells expressing control or silenced SRC (**Supplementary Fig. 2**), cell death in SRC-silenced cells treated with 50 μM etoposide was fully rescued by the addition of ZVAD-FMK (**Fig. 2d**), indicating that SRC silencing in this senescence paradigm sensitized cells to undergo apoptotic cell death. Furthermore, analysis of Caspase 3/7 activity in etoposide-treated cells (50 μM) by a luminescence assay (Methods) revealed that SRC silencing increased caspase activity compared to control cells (**Fig. 2e**) and that the increased caspase activity was fully rescued by addition of ZVAD-FMK. In short, SRC contributed to maintaining a senescence phenotype and avoiding apoptosis in response to etoposide-induced damage.

We then asked whether the effect of SRC in promoting senescent-cell survival might be linked to its kinase activity. We generated viral vectors that expressed a constitutively active (CA) form of human SRC (Y530F), hereafter 'CA-SRC', where a substitution of tyrosine 530 to phenylalanine (Y530F) produces constitutive phosphorylation of the SRC-activating residue Y418[16,17]. We utilized the same system to generate a dominant-negative (DN) mutant construct of human SRC featuring K298M/Y530F mutations; hereafter 'DN-SRC'. These viral vectors also have a C-terminal MYC tag, a doxycycline-inducible promoter, and an IRES-driven RFP reporter to track their expression in cells. After transducing cells with the lentiviral particles (**Fig. 2f**), we tested whether expression of CA-SRC and DN-SRC influenced the proportion of apoptotic cells in etoposide-treated cells. As shown, CA-SRC expression significantly increased the survival of cells treated with 200 μM etoposide, while expression of DN-SRC reduced the viability of cells treated with 50 μM etoposide (**Fig. 2g**). Transduction efficiency was monitored by immunoblot analysis of the MYC tag (**Fig. 2h**) and by tracking RFP fluorescence after 72 h (**Supplementary Fig. 3a**). Importantly, no changes were observed in proliferating cells when SRC mutants were overexpressed (**Supplementary Fig. 3b**). These data support the notion that SRC activity elicits a pro-survival influence in cells responding to senescence-inducing genotoxic stress.

**Pharmacologic inhibition of SRC activity orients cells toward apoptosis instead of senescence**

We used commercially available SRC inhibitors to study if they could reproduce the effects observed when silencing SRC. We treated cells simultaneously with 50 μM etoposide and SRC inhibitors PP1, PP2, Dasatinib, or AZM 475271 (**Fig. 3a**). As shown (**Figs. 3b, c**), all SRC inhibitors reduced the viability of cells treated with 50 μM etoposide, recapitulating the effects seen when SRC was silenced. In the absence of etoposide, none of the inhibitors reduced cell viability significantly by 48 h, compared to untreated controls, although both Dasatinib and AZM 475271 reduced proliferation modestly in undamaged cells (**Supplementary Fig. 4a**). These observations agree with the known function of SRC as a transducer of growth signals from activated RTKs[10].

To further study if the effect of SRC inhibition can be expanded to other cellular systems, we tested human diploid WI-38 and BJ fibroblasts, commonly used to study cell senescence but distinct from IMR-90 fibroblasts[18]. Analysis of the thresholds of etoposide that induced senescence or apoptosis revealed that, like IMR-90 fibroblasts, WI-38 fibroblasts also underwent senescence with 50 μM etoposide (**Fig. 3d**); this phenotype was confirmed by increased SA-β-Gal staining (**Fig. 3e** and **Supplementary 4b**), decreased BrdU incorporation (**Fig. 3f**), as well as increased levels of *p16* and *IL6* mRNAs (**Fig. 3g**). Further treatment with PP1 and PP2, the two SRC inhibitors with the strongest effect in IMR-90 cells, significantly sensitized WI-38 cells to apoptotic cell death (**Fig. 3h**). This sensitization was specific for etoposide-treated cells, as untreated, proliferating WI-38 cells showed neither cell death nor decreased proliferation when treated with PP1 or PP2 (**Supplementary Fig. 4c**). BJ fibroblasts were significantly more sensitive to DNA damage caused by etoposide (**Fig. 3i**) and thus we utilized 25 μM etoposide to induce senescence, which was confirmed by SA-β-Gal staining, reduced BrdU incorporation, and increased levels of *p16* and *IL6* mRNAs (**Figs. 3j-l** and **Supplementary Fig. 4d**). Treating senescent BJ cells with PP1 and PP2 resulted in a dramatic increase in cell death, similar to the findings in IMR-90 and WI-38 fibroblasts (**Fig. 3m**), while untreated BJ cells were unaffected by SRC inhibitors (**Supplementary Fig. 4e**). Collectively, these results indicate that pharmacological inhibition of SRC could potentially offer a strategy to redirect cells with sublethal DNA damage from senescence to apoptosis.

**Essential factors drive dichotomous cell fate determination downstream of SRC signaling**

The fate of damaged cells is determined by a tightly regulated balance between pro-apoptotic and pro-survival proteins[15]. To gain further insight into the mechanisms underlying the cell fate determination during early senescence, we compared our earlier phosphoprotein survey with transcriptomic profiling of cells treated with 50 μM and 200 μM etoposide (GSE169037; token ajupausmfhmzfyh). Gene Set Enrichment Analysis (GSEA) associated with 200 μM etoposide treatment identified both apoptotic (Hallmark: Apoptosis) and p53 (Hallmark: p53 pathway) transcriptomic programs (**Fig. 4a**), in keeping with the role of p53 in controlling apoptotic cell death[19]. The most prominent mRNAs encoding anti-apoptotic proteins increased in senescence-committed cells but not in pro-apoptotic conditions (**Fig. 4b**),

as they might be key to triggering cell death when damage is excessive. Interestingly, only 2 out of the 14 mRNAs (box), encoding pro-survival proteins BIRC6 and BCL2L2, displayed that trend; BCL2L2 is an anti-apoptotic, senescence-associated protein belonging to the BCL2 pro-survival protein family usually targeted by senolytic drugs[6,7].

As shown (**Fig. 4c** and **Supplementary Fig. 5a**) RT-qPCR analysis confirmed the expression profiles of the main pro-apoptotic mRNAs regulated by p53 (*BBC3/PUMA*, *PMAIP1*, *BAX*, and *APAF1* mRNAs), as well as the pro-survival *BCL2L2*, *BIRC6*, and *BCL2L1* mRNAs; additionally, only *PUMA* and *PMAIP1* mRNAs increased robustly in cells treated with both 50 and 200 μM etoposide, while only *BCL2L2* mRNA increased selectively by 50 μM but not by 200 μM etoposide. Western blot analysis revealed that the levels of PUMA (NOXA), PMAIP1, BCL2L2 (BCL-W) and BCL2L1 (BCL-XL), reflected the changes in mRNA levels (**Fig. 4d**).

To directly test if PUMA or PMAIP1 reduced IMR-90 cell survival, we silenced them using specific siRNAs and 48 h later, we challenged cells with 200 μM etoposide. We found that silencing either *PUMA* or *PMAIP1* mRNAs partially but significantly reduced cell death caused by etoposide (**Fig. 4e,f**). Silencing these genes did not affect survival of proliferating cells (**Supplementary Fig. 5b,c**). Both BCL2L2 and BCL2L1 contributed to maintaining cell viability during senescence, as silencing them using dedicated siRNAs and challenging them 48 h later with 50 μM etoposide resulted in enhanced cell death (**Fig. 4g**,**h**). In a complementary experiment, treatment with ABT-737 (a senolytic agent that inhibits BCL2L1 and BCL2L2) diverted senescent cells towards apoptosis (**Supplementary Fig. 5d**). In proliferating cells, simply silencing *BCL2L1* mRNA reduced cell viability (**Supplementary Fig. 5e**); since silencing *BCL2L2* mRNA did not have this effect, we propose that BCL2L2 more specifically protects senescence-committed cells. We thus focused on PUMA and BCL2L2 as representative factors in the survival-apoptosis balance reached in early senescence. To test their direct impact on this balance, we studied if the death caused by BCL2L2 silencing might be rescued by simultaneously depleting PUMA. Notably, while BCL2L2 silencing decreased viability in cells treated with 50 μM etoposide, simultaneous silencing of PUMA partially prevented this reduction (**Fig. 4i**). Silencing PUMA alone had no effect on survival (**Fig. 4i**), and these silencing interventions did not affect proliferating cells (**Supplementary Fig. 5e**). These results suggest that pro-apoptotic PUMA and anti-apoptotic BCL2L2 directly contribute to the survival-apoptosis balance in the SRC-regulated response to etoposide in early senescence. Assessment of the *PUMA* and *BCL2L2* mRNA expression levels revealed that their abundance at 50 and 200 μM etoposide treatments diverged at 48 h (**Fig. 4j**), as cell fate began to be apparent. SRC phosphorylation remained higher in the 50 μM than in the 200 μM treatment groups, also starting to diverge after 24 h of etoposide treatment (**Fig. 4k**), suggesting potential coordination between SRC activation and the expression of cell fate proteins.

The phosphoarray data (**Fig. 1h**) were used to identify signaling pathways altered between senescence- and apoptosis-triggering conditions. By including all proteins differentially phosphorylated in both conditions to find central hub signaling proteins (PPI Hub Proteins app within EnrichR

platform)[20,21], the highest-ranking hub proteins aside from SRC family members were key signaling elements downstream of SRC, including MAPK1 (ERK2), MAPK3 (ERK1), AKT1 (AKT), MAPK8 (JNK1), MAPK14 (p38-alpha), and STAT3 (**Supplementary Fig. 5f**). Additionally, p53, also regulated by SRC, was one of the top proteins showing increased phosphorylation of a key inactivating residue, S315 (**Supplementary Fig. 1**). GSEA further suggested a strong association of p53 activation with 200 μM etoposide treatment, which was also confirmed by increased p53 protein levels (**Fig. 4l**), and increased levels of *PUMA* and *PMAIP1* mRNAs in this treatment group (**Fig. 4c**). Etoposide treatment strongly increased the phosphorylation of activating residues in the MAPKs (ERK1/2, p38, and JNK) and increased more modestly STAT3 phosphorylation with 50 μM etoposide only (**Fig. 4m**, **Supplementary Fig. 5g**). Both ERK1/2 and JNK demonstrated stronger increases of phosphorylation by 200 μM compared to 50 μM etoposide (**Fig. 4m**), while p38 showed the opposite pattern, with increased phosphorylation in senescence-committed cells and slightly decreased phosphorylation in apoptosis-committed cells. Although MAPKs play differing roles in regulating the apoptosis-survival balance[12], p38 was recently identified as a pro-survival signaling kinase in senescence[22], and was found to increase *BCL2L2* mRNA levels[23], and was the only MAPK showing activation in senescence-committed cells in our experiments (**Fig. 4m**). Phosphorylation of another pro-survival protein, AKT, was not observed in the 50 μM etoposide group, and was reduced with 200 μM etoposide[11]. Finally, STAT3 phosphorylation at Y705 increased modestly in senescence-committed and declined in apoptosis-committed IMR-90 cells. In sum, coordinated signaling through SRC, p53 and MAPKs, with ensuing gene expression programs, appears important for translating the cellular responses to DNA damage into cell fate determination.

**p53 repression and p38 activation by SRC promote pro-survival responses in early senescence**

To further evaluate the role of SRC in the differential response to etoposide, we silenced SRC using siRNAs. By 48 h of treatment with 50 μM etoposide, SRC silencing further elevated p53 levels, suggesting that SRC might prevent an excessive rise in p53 levels (**Fig. 5a**). Moreover, silencing SRC decreased p38 phosphorylation, while it triggered a robust increase in ERK1/2 phosphorylation and a modest increase in phosphorylation of JNK and STAT3 (**Fig. 5b** and **Supplementary Fig. 5h**), suggesting that SRC influences these signaling cascades in senescent cells. SRC silencing did not affect AKT status, indicating that these two kinases are not closely related in early senescence. SRC silencing in cells treated with 50 μM etoposide increased p53 levels and diminished p38 activation, mirroring a pro-apoptotic pattern, and suggesting that SRC might act early to influence whether the cellular response is geared towards apoptosis or survival.

When SRC was silenced, the levels of *PUMA* mRNA (**Fig. 5c**) and *PMAIP1* mRNA (**Supplementary Fig. 5i**) increased dramatically in cells exposed to 50 μM etoposide, while *BCL2L2* mRNA levels decreased (**Fig. 5c**), and *BCL2L1* mRNA levels remained unaffected (**Supplementary Fig. 5i**). SRC silencing affected PUMA and BCL2L2 protein levels similarly at the protein level (**Fig.**

**5d**). The fact that silencing SRC increased PUMA and reduced BCL2L2 suggests that SRC helps to implement a pro-survival program in cells treated with 50 μM etoposide.

To further test this hypothesis, we characterized the role of SRC in cell fate determination by using the CA-SRC (Y530F) driven by a doxycycline-inducible promoter. We treated cells with apoptosis-inducing etoposide (200 μM) and attempted to diminish cell death by ectopically expressing CA-SRC. Moderate overexpression of SRC was confirmed by measuring endogenous and MYC-tagged SRC levels by western blot analysis (**Fig. 5e**). Interestingly, CA-SRC increased p38 phosphorylation and reduced p53 levels as determined by western blot analysis, resembling the patterns observed after treatment with 50 μM etoposide. Analysis of *PUMA* and *BCL2L2* mRNA levels also revealed pro-survival trends if CA-SRC was expressed, despite treatment with 200 μM etoposide: *PUMA* mRNA levels declined and *BCL2L2* mRNA levels increased (**Fig. 5f**), and protein levels reflected these trends (**Fig. 5g**). In conclusion, SRC silencing reversed the pro-survival phenotype after 50 μM etoposide treatment, while CA-SRC expression partly rescued the pro-apoptotic response following 200 μM etoposide treatment. These results support the notion that SRC function modulates the cellular determination to undergo senescence or apoptosis.

Given the contribution of SRC to the pro-survival phenotype of senescent cells, we explored if SRC inhibitors could remove already-senescent cells. Analysis of the impact of PP1 and PP2 (5 μM, 48 h) revealed that SRC inhibitors more potently reduced cell viability in early-stage (48 h in 50 μM etoposide) than in late-stage (10 days in 50 μM etoposide) senescent cells (**Fig. 5h**). *PUMA* mRNA levels peaked after 24 h, while *BCL2L2* mRNA levels gradually increased and were maintained into late senescence (**Fig. 5i**), further supporting the view that the influence of SRC on gene expression programs occurs early after the onset of damage. As both PP1 and PP2 are more potent inhibitors of SRC than the established senolytic Dasatinib (**Fig. 3b**), PP1 and PP2 deserve further attention in senolytic therapy. Taken together, these findings indicate that SRC contributes to a senescent, pro-survival phenotype by maintaining reduced p53 activity and elevated p38 activity.

**SRC influence on viability is modulated by signaling through p38 and p53**

To assess the abundance of pro-apoptotic PUMA and pro-survival BCL2L2 as a function of SRC-regulated p53 and p38, we examined whether p38 inhibition or p53 activation reproduced the effects of SRC on apoptosis. We utilized two highly specific compounds: AL 8697, a potent and selective inhibitor of p38 (p38i)[24] and Nutlin-3a, a known disruptor of MDM2-p53 interactions that renders p53 stable and active (p53a)[25]. As shown, in the presence of 50 μM etoposide, treatment with p38i (AL 8697) or p53a (Nutlin-3a) (10 μM each) decreased cell viability compared to 50 μM etoposide alone (**Fig. 6a**). Each compound sensitized cells to apoptosis significantly less than SRC inhibitors (**Fig. 3a**). Inhibition of the other two MAPKs increased by SRC silencing, ERK1/2 and JNK (using U0126 and SP 600125, respectively, 10 μM each), revealed no change in cell viability in the presence of 50 μM etoposide (**Supplementary Fig. 6a**), further supporting a prominent role for p38 in maintaining viability

during early senescence. As SRC inhibition affects both p53 and p38, we tested the effect of combining p38i and p53a. Both pathways appear important as there was strong sensitization to apoptosis by 48 h in 50 μM etoposide relative to treatments with p38i or p53a alone, but comparable to the effect of SRC inhibitors PP1 or PP2 (**Fig. 6a**, **Supplementary Fig. 6b**).

We then assessed the impact of p53 and p38 on the production of PUMA and BCL2L2. In line with earlier reports (reviewed in Ref. 12), p38i reduced the abundance of *BCL2L2* mRNA, but not *PUMA* mRNA (**Fig. 6b**), while p53a increased the levels of *PUMA* mRNA, a transcriptional target of p53, but not the levels of *BCL2L2* mRNA. Protein analysis generally showed similar trends, although BCL2L2 levels decreased by p53a treatment when compared to etoposide-only treated cells (**Fig. 6c**). As expected, p38 inhibition prevented the phosphorylation of p38 target HSP27, and Nutlin-3a elevated total p53 levels. These results indicate that p53 activation during early senescence directly increases *PUMA* mRNA levels, while p38 activity augments *BCL2L2* mRNA levels. Importantly, combined p38i+p53a treatment further increased the levels of *PUMA* mRNA, encoding the pro-apoptotic protein PUMA, and prevented the increase in *BCL2L2* mRNA elicited by 50 μM etoposide only, thus suppressing a rise in the pro-survival protein BCL2L2. These results illustrate the change in gene expression programs driven by p53 and p38 as effectors of SRC-driven responses. These results further support the notion that SRC inhibition, rather than p53 activation or p38 inhibition alone, is more effective in shifting the cell response to damage from senescence to apoptosis.

To further examine a model whereby SRC mounts a pro-survival program, CA-SRC expression increased cell viability of cells treated with 200 μM etoposide, but this protection was significantly reversed by combined treatment with p38i+p53a (**Fig. 6e**). Accordingly, both the CA-SRC-elicited decrease in *PUMA* mRNA levels and rise in *BCL2L2* mRNA levels were reversed by the p38i+p53a combination (**Fig. 6e**). These results further support a model whereby SRC is a key sensor of the damage encountered by a cell. Sublethal damage activates SRC, which in turn inhibits p53 and activates p38, suppressing apoptosis and implementing a survival gene expression program (including low PUMA and high BCL2L2) that leads to senescence. Lethal damage only minimally activated SRC, in turn enabling p53 activation and p38 repression and mounting a gene expression program (high PUMA, low BCL2L2) that leads to apoptosis (**Fig. 6f**).

**Inhibiting SRC in mice prevents the accumulation of senescent cells in chemotherapy-induced senescence**

To evaluate the physiologic relevance of our findings, we tested the effectiveness of SRC inhibition in senescence versus apoptosis fates in an established *in vivo* mouse model of senescence[26], triggered by a single intraperitoneal injection of doxorubicin (**Fig. 7a**). While both etoposide and doxorubicin trigger DNA damage by inhibiting Topoisomerase II[27], we first tested the effectiveness of SRC inhibitors in diverting doxorubicin-induced senescence in IMR-90 cells to apoptotic cell death. Importantly, both PP1 and PP2 inhibitors reduced cell viability significantly when added simultaneously with senescence-

inducing doses of doxorubicin (**Fig. 7b**). SA-β-Gal staining and BrdU incorporation assays (**Supplementary Fig. 7a**) confirmed that SRC inhibition shifted the cellular response to doxorubicin from senescence to apoptosis, similarly to what was seen with etoposide. Thus, we were ready to take on mouse studies.

Mice were either left untreated or treated with a single dose of doxorubicin (10 mg/kg), and then given either vehicle (10% DMSO in PBS), PP1, or PP2 consecutively for five days (**Fig. 7a**); eight days after doxorubicin administration, mouse tissues were harvested for analysis. In lung, RT-qPCR analysis revealed increased levels of *p21* and *Il6* mRNAs, two senescence-associated transcripts known to be elevated in this model[26,28] (**Fig. 7c**). Remarkably, treatment with both SRC inhibitors reduced the increases seen in the Doxo-treated mice, bringing their levels significantly nearer to the control (except for p21 levels in mice that received PP1). Next, we monitored the accumulation of senescent cells by measuring p21-positive cells in lung sections. As shown by microscopy and counting p21-positive cells, treatment with doxorubicin significantly elevated the percentage of p21-positive cells in the lungs (**Fig. 7d,e**), but PP1 and PP2 treatments reduced this rise.

We expanded this analysis to other tissues where doxorubicin treatment significantly induces p21 expression, such as kidney and liver[28]; here too, p21-positive cells accumulated by eight days after doxorubicin exposure, but treatment with PP1 or PP2 prevented this accumulation (**Figs. 7e**, **Supplementary Fig. 7c,d**). Finally, to test if SRC inhibition following doxorubicin damage *in vivo* favored apoptosis instead of senescence, we performed TUNEL assays (Methods) on lung sections. Notably, TUNEL-positive cells were more abundant in mice that received doxorubicin than in untreated mice (**Fig. 7f**), but treatment with PP1 or PP2 led to an even higher proportion of TUNEL-positive cells within the lungs. These data suggest that, by favoring apoptotic cell death following DNA damage, SRC inhibition also prevents senescence *in vivo*.

## Discussion

There is intense interest in identifying strategies to eliminate senescent cells in order to improve health span and disease outcomes[4]. Given that senescent cells are selectively resistant to apoptotic cell death, elucidating the mechanisms that engender protection to senescent cells has become an area of intense effort. While our knowledge of senolysis has expanded in recent years, much remains to be elucidated, particularly at the molecular level[11,29]. Here, we describe the identification of a mechanism whereby cells responding to DNA damage levels capable of triggering senescence can be redirected to undergo apoptosis. Following DNA damage, early changes in expressed proteins are known to drive cell fate by shifting the balance between pro-apoptotic and pro-survival programs; these programs are largely controlled by proteins in the BCL2 family[15]. In this regard, pro-survival members of the BCL2 family (e.g., BCL2, BCL2L2, BCL2L1) promote senescence, while pro-apoptotic members of the BCL2 family (e.g., PUMA, PMAIP1) enhance cell death[6,7]. Delineating the different signaling pathways is complex, given that in many cases the upstream regulators are shared. For example, a major effector of both apoptosis and senescence, p53, transcriptionally induces expression of p21, which can protect against apoptosis[30] and pro-apoptotic proteins such as PUMA, PMAIP1, BAX, or APAF1[31]. Similarly, another key regulator, p38, can promote the expression of both pro-survival proteins (such as BCL2L2)[23] and pro-apoptotic proteins (e.g., PMAIP levels in the absence of p53[32]). In this study, we found that the protein kinase SRC is an upstream regulator of this balance between senescence and apoptosis. In response to etoposide treatment, SRC simultaneously decreased p53 signaling and increased p38 signaling. As a result, silencing or inhibiting SRC led to an increase in PUMA production (and other p53-dependent pro-apoptotic proteins) and a reduction in BCL2L2, tilting the response from senescence/survival to apoptosis.

### *SRC as a pro-survival factor in senescence*

Identified as a strong pro-survival protein[14], SRC belongs to a family of non-receptor tyrosine kinases that are usually activated in cancer and other stress conditions. Although we focused on genotoxic stress, SRC can also be activated by RTKs, integrins, and increased oxidative stress levels[33]. Despite its prominent role in stress response programs, SRC was not previously linked to the balance between pro-survival and pro-apoptotic pathways that characterize the senescence response. Our results provide further evidence for the view that SRC activation following sublethal DNA damage promotes cell survival, and that this function relies on the coordination of p53 and MAPK signaling at an early point that defines the ensuing stress response[12,34]. Importantly, it complements earlier observations[35] reporting that signaling through integrins (α6β4), SRC, and AKT conferred survival in response to ionizing radiation. It also provides molecular context to an earlier report identifying SRC as a suppressor of apoptosis in senescent cells[36].

***Inhibition of p53 by SRC***

In the pro-apoptotic arm of our study, 200 μM etoposide increased several p53-dependent genes. Although the influence of p53 on lethal stress signals is quite complex, there is ample support for the notion that p53 levels dictate the decision between cell senescence and apoptosis[19], mediated by the broad range of transcriptionally regulated genes, including some that promote apoptosis (*PMAIP1/NOXA* and *BAX*) and others that prevent it (*PUMA*)[37]. In keeping with evidence that SRC inhibits p53 function directly, our phosphoprotein array data revealed that one of the top five most phosphorylated residues in senescence-committed cells was p53 S315, which promotes p53 proteasomal degradation by enhancing its interaction with MDM2[38]. This phosphorylation of p53 may be caused by AURKA (Aurora kinase A), a direct SRC substrate[38] or indirectly by SRC phosphorylation of CDK1, which in turn phosphorylates p53 S315[39, 40]. Aside from AURKA and CDK1, SRC phosphorylates HIPK2, which is then unable to bind p53 and this leads to decreased p53 activity[41]. SRC can also promote p53 degradation by disturbing the interaction between protein phosphatase (PP)2A and MDM2[42]. In sum, SRC activation decreases p53 function through many paths, and we have found that the SRC-mediated tempering of p53 levels is essential for favoring senescence over apoptosis. Previous studies examining different times and sources of DNA damage reported that cells restrain p53 induction through PKC activation[43], which often activates SRC[13].

***Activation of p38 by SRC***

To promote the survival of senescent cells, SRC function relies on p38 activity. In keeping with evidence that SRC induces p38 signaling, silencing SRC reduced p38 phosphorylation and lowered *BCL2L2* mRNA levels. *BCL2L2* mRNA levels are tightly regulated, in part by the transcription factors MEF2, ETS1/2, C/EBP, and NF-κB[44]. We found that *BCL2L2* mRNA levels increased by p38 signaling[23], but did not identify a specific transcription factor. Despite its complex influence on survival and apoptosis, p38 has been found to mainly promote cell viability in non-transformed cells[45]. In senescence, p38 favors cell survival by promoting autophagy[22], and perhaps by activating pathways such as those that increase NF-κB activity[46] or augment p21 expression levels[47]. Finally, active p38 can prevent cell death by inhibiting signaling through JNK[48], a pro-apoptotic MAPK. SRC can also activate p38 via traditional signal transduction from SRC to p38[10] or by the SRC-RAC1 signaling cascade[49]. Additionally, GADD45 proteins also contribute to the coordinated response to DNA damage and have been linked to p38 activation by SRC[42,50].

***Targeting SRC in senolytic strategies***

Our results point to SRC as a promising target to prevent the accumulation of senescent cells. Although SRC is widely expressed and active in homeostatic conditions, SRC activity increases in response to stress conditions[33,51,52]. Furthermore, SRC hyperactivation is common in cancer cells, and therefore strategies directed at SRC have been studied extensively in cancer treatment[14]. Moreover, Dasatinib, an

inhibitor of SRC and other kinases, was included in some of the first cocktails (Quercetin+Dasatinib) reported to selectively eliminate senescent cells[53]. Dasatinib was less effective than SRC inhibitors PP1 or PP2 in sensitizing cells to apoptosis, suggesting that current senolytics might be optimized for more efficient reduction of senescent cell viability. It is important to point out that SRC inhibition by PP1 or PP2 was more effective in reducing viability at early rather than late phases of senescence, although we did not directly compare this effect with Dasatinib or other established senolytics. In sum, although SRC-specific inhibitors effectively reduced viability during early senescence, more evidence is required to determine their efficacy during late-stage senescence.

Senescence can be beneficial in some contexts, but there are many scenarios in which senescence is highly detrimental. Chemotherapy-induced senescence of non-malignant cells is an example of cellular senescence that has been proven quite harmful[26]. Another example of deleterious senescence is the systemic reaction to the transplantation of organs[54,55]. Preventing the accumulation and deleterious impact of senescent cells could be alleviated with SRC inhibitors, potentially improving therapeutic outcomes such as renal transplantation[56]. Moreover, senescence of liver stellate cells from young mice prevents fibrosis[57], while their accumulation with age promotes steatosis[58]. An increased proportion of senescent hepatocytes drives liver fibrosis[59] and prevention of senescence within liver of adult mice enhances liver regeneration after partial hepatectomy[60] or acetaminophen poisoning[61]. It remains to be seen whether senescent cells improve or worsen the liver response to injury[62], although treatment with SRC inhibitors improved liver injury outcomes in senescence-related processes such as fibrosis, steatosis, and regeneration[63-65]. In this regard, the finding that SRC inhibitors prevented the accumulation of senescent cells in mouse lung, liver, and kidney after treatment with doxorubicin (**Fig. 7**), while it increased apoptosis in this model, suggests that interventions directed at SRC deserve direct consideration within efforts to exploit vulnerabilities in senescent cells for therapeutic benefit.

## Acknowledgements

This work was funded in its entirety by the National Institute on Aging Intramural Research Program of the National Institutes of Health.

## References


1. Gorgoulis, V. et al. Cellular Senescence: Defining a Path Forward. *Cell* **179,** 813-827 (2019).

2. McHugh, D. & Gil, J. Senescence and aging: Causes, consequences, and therapeutic avenues. *J. Cell Biol.* **217,** 65-77 (2018).

3. Lopez-Otin, C., Blasco, M. A., Partridge, L., Serrano, M., & Kroemer, G. The hallmarks of aging. *Cell* **153,** 1194-1217 (2013).

4. Di Micco, R., Krizhanovsky, V., Baker, D. & d'Adda di Fagagna, F. Cellular senescence in ageing: from mechanisms to therapeutic opportunities. *Nat. Rev. Mol. Cell. Biol.* **22,** 75-95 (2021).

5. Childs, B. G., Baker, D. J., Kirkland, J. L., Campisi, J. & van Deursen, J. M. Senescence and apoptosis: dueling or complementary cell fates? *EMBO Rep.* **15,** 1139-1153 (2014).

6. Yosef, R. et al. Directed elimination of senescent cells by inhibition of BCL-W and BCL-XL. *Nat. Commun.* **7,** 11190 (2016).

7. Chang, J. et al. Clearance of senescent cells by ABT263 rejuvenates aged hematopoietic stem cells in mice. *Nat. Med.* **22,** 78-83 (2016).

8. Baar, M. P. et al. Targeted apoptosis of senescent cells restores tissue homeostasis in response to chemotoxicity and aging. *Cell* **169,** 132-147 e116 (2017).

9. Ochoa, D. et al. The functional landscape of the human phosphoproteome. *Nat. Biotechnol.* **38,** 365-373 (2020).

10. Roskoski, R. Jr. Src protein-tyrosine kinase structure, mechanism, and small molecule inhibitors. *Pharmacol Res.* **94,** 9-25 (2015).

11. Soto-Gamez, A., Quax, W. J. & Demaria, M. Regulation of Survival Networks in Senescent Cells: From Mechanisms to Interventions. *J. Mol. Biol.* **431,** 2629-2643 (2019).

12. Anerillas, C., Abdelmohsen, K. & Gorospe, M. Regulation of senescence traits by MAPKs. *Geroscience* **42,** 397-408 (2020).

13. Anguita, E. & Villalobo, A. Src-family tyrosine kinases and the Ca(2+) signal. *Biochim Biophys. Acta Mol. Cell Res.* **1864,** 915-932 (2017).

14. Kim, L. C., Song, L. & Haura, E. B. Src kinases as therapeutic targets for cancer. *Nat. Rev. Clin. Oncol.* **6,** 587-595 (2009).

15. Singh, R., Letai, A. & Sarosiek, K. Regulation of apoptosis in health and disease: the balancing act of BCL-2 family proteins. *Nat. Rev. Mol. Cell. Biol.* **20,** 175-193 (2019).

16. Miyazaki, T. et al. Src kinase activity is essential for osteoclast function. *J. Biol. Chem.* **279,** 17660-17666 (2004).

17. Cai, H. et al. Differential transformation capacity of Src family kinases during the initiation of prostate cancer. *Proc. Natl. Acad. Sci. USA* **108,** 6579-6584 (2011).

18. Marthandan, S., et al. Conserved Senescence Associated Genes and Pathways in Primary Human Fibroblasts Detected by RNA-Seq. *PLoS One* **11,** e0154531 (2016).

19. Hafner, A., Bulyk, M. L., Jambhekar, A. & Lahav, G. The multiple mechanisms that regulate p53 activity and cell fate. *Nat. Rev. Mol. Cell. Biol.* **20,** 199-210 (2019).

20. Chen, E. Y. et al. Enrichr: interactive and collaborative HTML5 gene list enrichment analysis tool. BMC *Bioinformatics* **14,** 128 (2013).

21. Kuleshov, M. V. et al. Enrichr: a comprehensive gene set enrichment analysis web server 2016 update. *Nucleic Acids Res.* **44,** W90-97 (2016).

22. Slobodnyuk, K. et al. Autophagy-induced senescence is regulated by p38alpha signaling. *Cell Death Dis.* **10,** 376 (2019).

23. Danckwardt, S. et al. p38 MAPK controls prothrombin expression by regulated RNA 3' end processing. *Mol. Cell* **41,** 298-310 (2011).

24. Aiguade, J. et al. Novel triazolopyridylbenzamides as potent and selective p38alpha inhibitors. *Bioorg. Med. Chem. Lett.* **22,** 3431-3436 (2012).

25. Efeyan, A. et al. Induction of p53-dependent senescence by the MDM2 antagonist nutlin-3a in mouse cells of fibroblast origin. *Cancer Res.* **67,** 7350-7357 (2007).

26. Demaria, M. et al. Cellular Senescence Promotes Adverse Effects of Chemotherapy and Cancer Relapse. *Cancer Discov.* **7,** 165-176 (2017).

27. Nitiss, J. L. Targeting DNA topoisomerase II in cancer chemotherapy. *Nat. Rev. Cancer* **9,** 338-350 (2009).

28. Ohtani, N. et al. Visualizing the dynamics of p21(Waf1/Cip1) cyclin-dependent kinase inhibitor expression in living animals. *Proc. Natl. Acad. Sci. USA* **104,** 15034-15039 (2007).

29. Roy, A. L. et al. A Blueprint for Characterizing Senescence. *Cell* **183,** 1143-1146 (2020).

30. Yosef, R. et al. p21 maintains senescent cell viability under persistent DNA damage response by restraining JNK and caspase signaling. *EMBO J.* **36,** 2280-2295 (2017).

31. Fischer, M. Census and evaluation of p53 target genes. *Oncogene* **36,** 3943-3956 (2017).

32. Nys, K. et al. A p38(MAPK)/HIF-1 pathway initiated by UVB irradiation is required to induce Noxa and apoptosis of human keratinocytes. *J. Invest. Dermatol.* **130,** 2269-2276 (2010).

33. Sun, G. & Kemble, D. J. To C or not to C: direct and indirect redox regulation of Src protein tyrosine kinase. *Cell Cycle* **8,** 2353-2355 (2009).

34. Munoz-Espin, D. & Serrano, M. Cellular senescence: from physiology to pathology. *Nat. Rev. Mol. Cell. Biol.* **15,** 482-496 (2014).

35. Jung, S. H., et al. Integrin α6β4-Src-AKT signaling induces cellular senescence by counteracting apoptosis in irradiated tumor cells and tissues. *Cell Death Differ.* **26,** 245-259 (2019).

36. Ryu, S. J., Cho, K. A., Oh, Y. S. & Park, S. C. Role of Src-specific phosphorylation site on focal adhesion kinase for senescence-associated apoptosis resistance. *Apoptosis* **11,** 303-313 (2006).

37. Aubrey, B. J., Kelly, G. L., Janic, A., Herold, M. J. & Strasser, A. How does p53 induce apoptosis and how does this relate to p53-mediated tumour suppression? *Cell Death Differ.* **25,** 104-113 (2018).

38. Barretta, M. L. et al. Aurora-A recruitment and centrosomal maturation are regulated by a Golgi-activated pool of Src during G2. *Nat. Commun.* **7,** 11727 (2016).

39. Zhou, M., Meng, Z., Jobson, A. G., Pommier, Y. & Veenstra, T. D. Detection of in vitro kinase generated protein phosphorylation sites using gamma[18O4]-ATP and mass spectrometry. *Anal. Chem.* **79,** 7603-7610 (2007).

40. Nantajit, D. et al. Cyclin B1/Cdk1 phosphorylation of mitochondrial p53 induces anti-apoptotic response. *PLoS One* **5,** e12341 (2010).

41. Polonio-Vallon, T., Kirkpatrick, J., Krijgsveld, J. & Hofmann, T. G. Src kinase modulates the apoptotic p53 pathway by altering HIPK2 localization. *Cell Cycle* **13,** 115-125 (2014).

42. Yu, Y. et al. GADD45beta mediates p53 protein degradation via Src/PP2A/MDM2 pathway upon arsenite treatment. *Cell Death Dis.* **4,** e637 (2013).

43. Bluwstein, A., et al. PKC signaling prevents irradiation-induced apoptosis of primary human fibroblasts. *Cell Death Dis.* **4,** e498 (2013).

44. Hartman, M. L. & Czyz, M. BCL-w: apoptotic and non-apoptotic role in health and disease. *Cell Death Dis.* **11,** 260 (2020).

45. Igea, A. & Nebreda, A. R. The Stress Kinase p38alpha as a Target for Cancer Therapy. *Cancer Res.* **75,** 3997-4002 (2015).

46. Freund, A., Patil, C. K. & Campisi, J. p38MAPK is a novel DNA damage response-independent regulator of the senescence-associated secretory phenotype. *EMBO J.* **30,** 1536-1548 (2011).

47. Yosef, R. et al. p21 maintains senescent cell viability under persistent DNA damage response by restraining JNK and caspase signaling. *EMBO J.* **36,** 2280-2295 (2017).

48. Miura, H., Kondo, Y., Matsuda, M. & Aoki, K. Cell-to-Cell Heterogeneity in p38-Mediated Cross-Inhibition of JNK Causes Stochastic Cell Death. *Cell Rep.* **24,** 2658-2668 (2018).

49. Kim, M. J., et al. c-Src-p38 mitogen-activated protein kinase signaling is required for Akt activation in response to ionizing radiation. *Mol. Cancer Res.* **6,** 1872-1880 (2008).

50. Kim, J., Kang, D., Sun, B. K., Kim, J. H. & Song, J. J. TRAIL/MEKK4/p38/HSP27/Akt survival network is biphasically modulated by the Src/CIN85/c-Cbl complex. *Cell Signal.* **25,** 372-379 (2013).

51. Mahajan, K. & Mahajan, N. P. Cross talk of tyrosine kinases with the DNA damage signaling pathways. *Nucleic Acids Res.* **43,** 10588-10601 (2015).

52. Dandoulaki, M., Petsalaki, E., Sumpton, D., Zanivan, S. & Zachos, G. Src activation by Chk1 promotes actin patch formation and prevents chromatin bridge breakage in cytokinesis. *J. Cell Biol.* **217,** 3071-3089 (2018).

53. Zhu, Y., T. Tchkonia, T. Pirtskhalava, A. C. Gower, H. Ding, N. Giorgadze, A. K. Palmer, Y. Ikeno, G. B. Hubbard, M. Lenburg, et al. (2015). The Achilles' heel of senescent cells: from transcriptome to senolytic drugs. Aging Cell 14, 644-658.

54. Naesens, M. (2011). Replicative senescence in kidney aging, renal disease, and renal transplantation. Discov. Med. 11, 65-75.

55. Braun, H. et al. Cellular senescence limits regenerative capacity and allograft survival. *J. Am. Soc. Nephrol.* **23,** 1467-1473 (2012).

56. Wei, C. et al. Genomic Analysis of Kidney Allograft Injury Identifies Hematopoietic Cell Kinase as a Key Driver of Renal Fibrosis. *J. Am. Soc. Nephrol.* **28,** 1385-1393 (2017).

57. Krizhanovsky, V. et al. Senescence of activated stellate cells limits liver fibrosis. *Cell* **134,** 657-667 (2008).

58. Ogrodnik, M. et al. Cellular senescence drives age-dependent hepatic steatosis. *Nat. Commun.* **8,** 15691 (2017).

59. Jurk, D. et al. Chronic inflammation induces telomere dysfunction and accelerates ageing in mice. *Nat. Commun.* **2,** 4172 (2014).

60. Ritschka, B. et al. The senotherapeutic drug ABT-737 disrupts aberrant p21 expression to restore liver regeneration in adult mice. *Genes Dev.* **34,** 489-494 (2020).

61. Bird, T. G. et al. TGFbeta inhibition restores a regenerative response in acute liver injury by suppressing paracrine senescence. *Sci. Transl. Med.* **10** (2018).

62. Aravinthan, A. D. & Alexander, G. J. M. Senescence in chronic liver disease: Is the future in aging? *J. Hepatol.* **65,** 825-834 (2016).

63. Aspinall, R. J. et al. A Src family kinase inhibitor improves survival in experimental acute liver failure associated with elevated cerebral and circulating vascular endothelial growth factor levels. *Liver Int.* **31,** 1222-1230 (2011).

64. Lakhani, H. V. et al. Phenotypic Alteration of Hepatocytes in Non-Alcoholic Fatty Liver Disease. *Int. J. Med. Sci.* **15,** 1591-1599 (2018).

65. Seo, H. Y. et al. Src Inhibition Attenuates Liver Fibrosis by Preventing Hepatic Stellate Cell Activation and Decreasing Connetive Tissue Growth Factor. *Cells* **9** (2020).

66. Mootha, V. K. et al PGC-1alpha-responsive genes involved in oxidative phosphorylation are coordinately downregulated in human diabetes. *Nat. Genet.* **34,** 267-273 (2003).

67. Subramanian, A. et al. Gene set enrichment analysis: a knowledge-based approach for interpreting genome-wide expression profiles. *Proc. Natl. Acad. Sci. USA* **102,** 15545-15550 (2005).

## Methods

### Cell culture, treatment, and detection of SA-β-Gal

Human IMR-90 (ATCC), WI-38 (Coriell Institute), and BJ fibroblasts (ATCC) were cultured in Dulbecco's modified Eagle's medium (DMEM, Gibco) supplemented with 10% heat-inactivated fetal bovine serum (FBS, Gibco), Penn/Strep (Gibco), Sodium Pyruvate (Gibco), and non-essential amino acids (Gibco) in a 5% CO2 incubator. Cells were maintained at low population doubling levels (PDL) ranging between PDL15 and PDL25. Every control condition included equivalent concentrations of vehicle (DMSO). Doxycycline (1 μg/ml) was refreshed every 24 h. Etoposide and doxorubicin were added to the media as indicated every 3 days. The remaining drugs utilized were refreshed every 48 hours. The drugs used are listed (**Supplementary Table 2**).

Cells were transfected with RNAiMAX (Invitrogen) following the manufacturer's instructions. Using RNAiMAX, 50% confluent cells were transfected with ON-TARGETplus SMARTPool (Dharmacon) non-targeting siCtrl (Catalog ID: D-001810-10-05), siSRC (Catalog ID: L-003175-00-0005), siBCL2L2 (Catalog ID: L-004384-00-0005), siBCL2L1 (Catalog ID: L-003458-00-0005), siPUMA/BBC3 (Catalog ID: L-004380-00-0005), and siPMAIP1 (Catalog ID: L-005275-00-0005) siRNAs at a final concentration of 25 nM. Forty-eight hours later, additional treatments were initiated as indicated. Viability was assessed by cell counting and represented as the percentage of remaining cells compared to the number of cells present at the beginning of the experiment. Senescence-associated β-galactosidase (SA-β-Gal) activity was evaluated following the manufacturer's instructions (Cell Signaling Technology). All cell counts were performed manually by using ImageJ and performed in at least three independent replicates. From each replicate, 3 fields were counted.

### Lentiviral vectors

Lentiviral constructs were commercially produced by Cellecta. Either constitutively active SRC (CA-SRC, human SRC Y530F) or dominant-negative SRC (DN-SRC, human SRC K298M/Y530F) were cloned into Cellecta-pTMONRB-TRE-MCS-I2-TagRFP-EFS-rtTA-2A-Blast lentiviral plasmid with a C-terminal MYC-tag. The mutations generated were based on extensive literature on SRC structure and function[16,17]. Lentiviral constructs were also packaged by Cellecta and transduced at a 3 MOI with polybrene (Millipore).

### RT-qPCR analysis

Samples (tissues or cells) were lysed in Tri-Reagent (Invitrogen). The extracted aqueous phase was processed with the QIAcube (Qiagen) to purify total RNA, which was then subjected to reverse transcription (RT) to create cDNA using Maxima reverse transcriptase (Thermo Fisher Scientific) and random hexamers. Following RT, quantitative (q)PCR analyses were performed using SYBR Green

mix (Kapa Biosystems). Relative expression was determined by the $2^{-\Delta\Delta Ct}$ method and normalized to *ACTB* mRNA levels. The primers used were as follows, each forward (F) and reverse (R): GCACAGAGCCTCGCCTT and GTTGTCGACGACGAGCG for human *ACTB* mRNA; GTTACGGTCGGAGGCCG and GTGAGAGTGGCGGGGTC for human *P16* mRNA; AGTGAGGAACAAGCCAGAGC and GTCAGGGGTGGTTATTGCAT for human *IL6* mRNA; GACCTCAACGCACAGTACGAG and AGGAGTCCCATGATGAGATTGT for human *BBC3/PUMA* mRNA;
GATGGTGGCCTACCTGGAGA and AGAGCTGTGAACTCCGCCCA for human *BCL2L2* mRNA; CCCGAGAGGTCTTTTTCCGAG and CCAGCCCATGATGGTTCTGAT for human *BAX* mRNA; AAGGTGGAGTACCACAGAGG and TCCATGTATGGTGACCCATCC for human *APAF1* mRNA; GAGCTGGTGGTTGACTTTCTC and TCCATCTCCGATTCAGTCCCT for human *BCL2L1* mRNA; GAGCGGCTCCAGATTGTCAA and CTGGGGATGTAGCCTGTCTGT for human *SRC* mRNA; CAGCAGCTCTTATCAGCATGT and AACTGTGGCCCACTTAGCAAC for human *BIRC6* mRNA; ACCAAGCCGGATTTGCGATT and ACTTGCACTTGTTCCTCGTGG for human *PMAIP1* mRNA: GAGCGGCTCCAGATTGTCAA and CTGGGGATGTAGCCTGTCTGT for human *SRC* mRNA; TTCTTTGCAGCTCCTTCGTT and ATGGAGGGGAATACAGCCC for mouse *Actb* mRNA; TTGCCAGCAGAATAAAAGGTG and TTTGCTCCTGTGCGGAAC for mouse *Cdkn1a* mRNA; and ACCAGAGGAAATTTTCAATAGGC and TGATGCACTTGCAGAAAACA mouse *Il6* mRNA.

**Western blot analysis**

Protein extracts were obtained by lysing cells with a denaturing buffer containing 2% sodium dodecyl sulfate (SDS) (Sigma-Aldrich) in 50 mM HEPES. After boiling and sonication, whole-cell protein extracts were size-fractionated through polyacrylamide gels and transferred to nitrocellulose membranes (Bio-Rad). Membranes were blocked with 5% non-fat dry milk and immunoblotted. Specific primary antibodies recognized total p38 MAPK (Cell Signaling, Ref. 9212S), phosphorylated p38 MAPK (T180/Y182) (Biolegend, Ref. 903501), total SRC (Cell Signaling, Ref. 2108S), phosphorylated SRC (Y416) (Cell Signaling, 6943S), total SAPK/JNK Antibody (Cell Signaling, 9252S), phosphorylated SAPK/JNK (T183/Y185) (81E11) (Cell Signaling, Ref. 4668S), total ERK1/2 (Cell Signaling, 4695S), phosphorylated ERK1/2 (T202/Y204) (Biolegend, 675502), total AKT (pan) (40D4) (Cell Signaling, 2920S), phosphorylated AKT (Ser473) (Cell Signaling, 4060S), total STAT3 (124H6) (Cell Signaling, 9139T), phosphorylated STAT3 (Y705) (D3A7) XP® (Cell Signaling, 9145S), p53 (DO-1) (Cell Signaling, 18032S), ACTB (β-Actin C4) (Santa Cruz Biotechnology, sc-47778), cleaved CASP3 (Caspase-3) (Asp175) (Cell Signaling, 9661S), PUMA (Cell Signaling, 98672S), PMAIP1/NOXA (Cell Signaling, 4766S), BCL2L1/BCL-xL (Cell Signaling, 2764S), and BCL2L2/BCL-w (Cell Signaling, 2724S). After incubation with the appropriate secondary antibodies conjugated with horseradish peroxidase (HRP; Jackson Immunoresearch), the chemiluminescent signals were detected by using the Chemidoc system (Biorad).

**BrdU incorporation**

Forty thousand cells were seeded in 24-well plates and incubated with 5-bromo-2′-deoxyuridine (BrdU) diluted in DMEM media with 10% FBS for 24 h. BrdU incorporation was measured following the manufacturer's protocol (Cell Signaling Technology). Briefly, cells were fixed and denatured prior to the addition BrdU mouse mAb and BrdU was detected the BrdU using the GloMax plate reader (Promega).

**Caspase 3/7 activity**

Apoptosis was monitored by measuring Caspase 3/7 activity using the Caspase-Glo 3/7 Assay System (Promega). Briefly, Caspase-Glo® 3/7 solution at 25 ºC was added directly to each well. The plate was then shaken vigorously for 30 sec and incubated at 25 ºC in the dark for 30 to 180 min. Luminescence was then measured using a GloMax plate reader (Promega).

**Phosphoarray analysis**

The Phospho Explorer Antibody Array (Full Moon Biosystems) platform was used to assess the phosphorylation status of protein samples in different conditions tested (n=2 samples per condition). Cell lysates were prepared using the Protein Extraction Kit and lysates were biotinylated and incubated on the array slides for 2 h at 25 ºC. After washes following the manufacturer's protocol, the array slides were incubated with Cy3-Streptavidin for 45 min at 25 ºC. The arrays were sent to the manufacturer for signal extraction. The data were normalized to the median signal intensity of all signals on the slide. Fold changes among samples were calculated, and those under 1.25-fold and above 0.8-fold were excluded from the final dataset. The complete dataset is provided as **Supplementary Table 1**.

**Transcriptomic analysis**

RNA was extracted with RLT buffer (Qiagen) and purified using the QIAcube system (Qiagen). RNA quality and quantity were determined using the Agilent Bioanalyzer RNA6000 Chip (Agilent, Santa Clara, CA). Total RNA (200 ng) was labeled according to the manufacturer′s recommendations using a QuickAmp Labeling Kit (Agilent 5190-2305). Cy3-labeled cRNA (600 ng) was hybridized for 17 h to Agilent SurePrint G3 Human 8x60K V3 microarrays, rinsed, and scanned at 3 µm using an Agilent SureScan scanner. Hybridization intensity data were extracted using Agilent′s Feature Extraction Software. Quantile-normalized data was further used for the subsequent analyses. GSEA analysis was performed as previously described, using non-Log2 transformed data[66,67]. The heat map represents relative differences (Log2), displayed by raw Z score calculations. The complete microarray dataset is provided in GSE169037 (token: ajupausmfhmzfyh).

**Mice and doxorubicin-induced *in vivo* senescence**

All mouse work, including the import, housing, experimental procedures, and euthanasia, were approved by the Animal Care and Use Committee (ACUC) of National Institute on Aging (NIA). C57BL/6J mice (Stock #000664) 10- to 12-weeks-old were imported from the Jackson Laboratory (Bar Harbor, ME), and housed in the animal facility in NIA. Mice were provided standard chow *ad libitum* and maintained under a 12:12 h light/dark cycle. Systemic cellular senescence was introduced by treating mice with doxorubicin, as described[26]. Briefly, a single dose of doxorubicin (10 mg/kg) and/or SRC inhibitor was injected intraperitoneally and organs (lung, kidney, liver) were collected.

**TUNEL assay and p21 immunofluorescence in tissue sections**

To prepare sections, mouse organs were fixed in 4% PFA (Paraformaldehyde) at 4 ºC for 16 h, followed by cryopreservation pretreatment in 30% sucrose for additional 16 h. The organs were embedded in OCT (optimal cutting temperature) compound and frozen at -80 ºC, 16 h later, blocks were cut into 10-µm sections by using a Leica cryostat. Slide-mounted sections were dried out for 16 h at 25 ºC. Immunofluorescent detection of p21 was performed by permeabilizing sections with 0.1% TX-100 in PBS for 2 min at 25 ºC, blocking with 10% goat serum for 1 h at 25 ºC, and incubating with anti-p21 antibody (Abcam, [EPR18021], ab188224) in 10% goat serum for 16 h at 4 ºC. A fluorescent secondary antibody (Invitrogen, goat anti-Rabbit IgG (H+L) superclonal, Alexa Fluor 647) was then incubated in 10% goat serum for 1 h at 25 ºC and slides were mounted with ProLong Diamond Antipode Mountant with DAPI (Life Technologies) and coverslips. TUNEL assay (InSitu Cell Death Detection Kit, Fluorescein, Roche) was performed following manufacturer's instructions. Signals were collected using a fluorescence microscope (BZ-X Analyzer, Keyence) and analyzed with ImageJ. Scale bars, 50 µm.

**Statistical Analysis**

Data are presented as the means ± standard deviation (S.D.) of at least n=3 independent experiments. Significance was established using two-tailed Student's t test (*, $P < 0.05$, **, $P < 0.01$, ***, $P < 0.001$).

**Data availability**

The microarray data have been deposited in GSE169037 (reviewer token: ajupausmfhmzfyh).

## Figure Legends

**Figure 1. Pro-survival signaling in senescence-committed cells implicate the SRC pathway. a** Schematic representation of the experimental strategy used to determine the threshold of etoposide required to induce senescence or apoptosis. **b** Timeline of etoposide treatment of proliferating IMR-90 fibroblasts. **c** Percentage of live cells, as assessed by direct cell counts, following etoposide treatment as explained in (b); green arrow indicates the time point selected for subsequent experiments. **d** Representative micrographs of SA-β-gal staining of cells 10 days after either no treatment or treatment with 50 μM etoposide. Scale bar, 100 μm. *Right*, Quantification of the percentage of SA-β-gal-positive cells in each condition. **e** Measurement of BrdU incorporation in cells that were either left untreated or treated for 10 days with 50 μM etoposide as explained in (B). **f** RT-qPCR assessment of the levels of *p16* and *IL6* mRNAs in cells that were either untreated or treated for 10 days with 50 μM etoposide as explained in (B); data were normalized to *ACTB* mRNA levels. **g** STRING analysis of proteins differentially phosphorylated 48 h after treating cells with 50 or 200 μM etoposide. The graph represents the number of protein interactions identified for the indicated protein. **h** Heat map representation of the protein sites with significantly changed phosphorylation status between 50 and 200 μM etoposide treatment (see also **Supplementary Fig. 1**; data are means of n=2 per condition). Arrow indicates SRC phosphorylated at Y418. *Left*, color representation of fold changes. **i** Representative Western blot analysis of Phospho-SRC (Y418), total SRC, cleaved Caspase3 (CASP3), and loading control β-Actin (ACTB) of whole-cell lysates from IMR-90 cultures that were either left untreated or treated with 50 or 200 μM etoposide. Graphs in **c-f** display the mean values ± SD of n=3 experiments; significance (*, $P < 0.05$, **, $P < 0.01$, ***, $P < 0.001$) was determined by using two-tailed Student's t-test.

**Figure 2. Modulation of SRC activity in IMR-90 cells controls cell fate after etoposide treatment. a** Levels of SRC protein, as assessed by Western blot analysis (top) and *SRC* mRNA, as assessed by RT-qPCR analysis (bottom) in IMR-90 fibroblasts that were either left untreated or treated for 48 h with 50 μM etoposide. **b** Representative micrographs of IMR-90 fibroblasts transfected with either control siRNA (siCtrl) or siRNA directed at *SRC* mRNA (siSRC), and were either left untreated or treated with etoposide 50 μM for 48 h. **c** Cells were treated as described in (B); live cells were counted after 48 hours. **d, e** Cells were transfected with the siRNAs shown; 48 h later they were either left untreated or treated with the Caspase inhibitor Z-VAD-FMK in the presence of 50 μM etoposide; 48 h later, cell viability was assessed by direct cell counting of remaining cells (d), and Caspase 3/7-dependent luciferase activity was assessed in each group (e). **f-h** Schematic representation of the constitutively active (CA) and dominant-negative (DN) SRC lentiviral constructs generated (f). IMR-90 cells were transduced with CA-SRC or DN-SRC (g) and induced by doxycycline (1 μg/ml) in cells treated with either 200 μM or 50 μM (g) etoposide. Cell viability was monitored by direct cell counting and plotted

as a percentage of cells at time 0. Western blot analysis of the levels of MYC-tagged SRC mutants (see also **Supplementary Fig. 3a**) after 72 h in the presence of doxycycline; ACTB was included as a loading control (h). Graphs in a, c-e, g represent the mean values ± SD of n=3 experiments; significance (*, $P < 0.05$, **, $P < 0.01$, ***, $P < 0.001$) was determined by using two-tailed Student's t-test.

**Figure 3. Inhibition of SRC kinase activity skews towards apoptosis instead of senescence. a** Schematic describing the schedule of treatments with SRC inhibitor and etoposide. **b** Cell viability was measured by direct cell counting 48 h after simultaneous treatment of IMR-90 cells with 50 μM etoposide and either no further treatment or treatment with SRC inhibitors. **c** Representative micrographs 48 h after simultaneous treatment of IMR-90 fibroblasts with 50 μM etoposide and the indicated SRC inhibitors. Scale bars, 100 μm. **d** Cell viability was assessed in each treatment group by direct counting of WI-38 cells at the times and etoposide concentrations shown. **e-g** Cellular senescence at day 10 was assessed by SA-β-gal staining (e), BrdU incorporation (f), and RT-qPCR analysis of the levels of senescence markers *p16* and *IL6* mRNA, normalized to the levels of *ACTB* mRNA (g). **h** Viability was determined by direct counting of human WI-38 fibroblasts treated with 50 μM etoposide in the absence or presence PP1 or PP2. **i** Percentages of live cells as assessed by direct counting of human BJ fibroblasts treated with different etoposide doses. **j-l** Assessment of senescence in BJ fibroblasts at day 10 of treatment with 25 μM etoposide by SA-β-gal staining (j), BrdU incorporation (k), and RT-qPCR assessment of the levels of *p16* and *IL6* mRNAs (l). **m** Cell viability after joint treatment with 25 μM etoposide and PP1 or PP2 as described for IMR-90 cells (a) and WI-38 cells (b, h). In panels (b, d, f, g, i, j), significance was assessed by two-tailed Student's t-test. Graphs represent the mean values ± SD of n=3 experiments; significance (*, $P < 0.05$, **, $P < 0.01$, ***, $P < 0.001$) was determined by using two-tailed Student's t-test.

**Figure 4. Essential genes for cell fate determination are regulated by signaling through SRC. a, b** GSEA analysis plots (a) and heat map (b) depicting transcriptomic (microarray) analysis of mRNAs encoding pro-apoptotic (a) or pro-survival (b) proteins in cells that were either left untreated (-) or treated for 48 h with 50 or 200 μM etoposide. Data shown in (b) are raw Z Score of the Log2-normalized expression values for each transcript (n=3 per condition). **c** Validation of the top microarray target transcripts, *PUMA, PMAIP1, BCL2L2*, and *BCL2L1* mRNAs by RT-qPCR analysis (see also **Supplementary Fig. 5a**). **d** Representative Western blot analysis of the levels of PUMA, PMAIP1, BCL2L2, and BCL2L1 proteins in cells treated as indicated in (a). **e** RT-qPCR assessment of the levels of *PUMA* and *PMAIP1* mRNAs 72 h after transfection with specific siRNAs (normalized to *ACTB* mRNA levels). **f** Cells were transfected with either siCtrl, siPUMA, or siPMAIP1 siRNAs and treated with 200 μM etoposide; cell viability was assessed by direct cell counting at the times indicated (see also **Supplementary Fig. 5b**). Significant differences are indicated above the curves (siPUMA vs

siCtrl), and below the curves (siPMAIP1 vs siCtrl). **g** RT-qPCR assessment of the levels of *BCL2L2* and *BCL2L1* mRNAs 72 h after transfection with specific siRNAs (normalized to *ACTB* mRNA levels). **h** Cells were transfected with either siCtrl, siBCL2L2, or siBCL2L1 siRNAs and treated with 50 μM etoposide; cell viability was assessed by direct cell counting at the indicated times (see also **Supplementary Fig. 5e**). Significant differences are indicated above the curves (siBCL2L1 vs siCtrl), and below the curves (siBCL2L2 vs siCtrl). **i** Cells were transfected with either siCtrl, siPUMA, siBCL2L2, or siPUMA+siBCL2L2 siRNAs and treated with 50 μM etoposide; cell viability was assessed by direct cell counting at the indicated times (see also **Supplementary Fig. 5e**). Significant differences are indicated. **j** Influence of etoposide (50 or 200 μM) on the time-dependent abundance of *PUMA* and *BCL2L2* mRNAs, as assessed by RT-qPCR analysis (normalized to *ACTB* mRNA levels). **k** Representative Western blot analysis of the levels of SRC, phosphorylated SRC (Y418), and loading control ACTB in IMR-90 cells treated with 50 or 200 μM etoposide for the times indicated. Values below the blot represent the means ± SD from densitometric quantification of signals in n=3 experiments. **l** Heat map representation (*top*) of quantified densitometry signals from p53 by Western blot analysis (bottom) in IMR-90 cells that were either left untreated or treated with 50 μM or 200 μM etoposide for 48 hours. **m** Heat map representation of the quantified densitometry signals on western blots detecting phosphorylated protein relative to corresponding total protein. Representative Western blots are in **Supplementary Fig. 5g**. Data are represented as Log2 of the normalized values. Graphs (c, e-j) represent the means ± SD from n=3 experiments; significance (*, $P < 0.05$, **, $P < 0.01$, ***, $P < 0.001$) was determined by using two-tailed Student's t-test.

**Figure 5. SRC represses p53 and promotes p38 signaling to favor survival in early senescence. a** Heat map representation of p53 levels (*top*) quantified by densitometry from signals on western blots (*bottom*, representative panel) in IMR-90 cells transfected with siCtrl or siSRC siRNAs, either untreated or treated with 50 μM Etoposide for 48 h. **b** Heat map representation of densitometry quantification of signals on western blots detecting phosphorylated residues, normalized to protein levels assessed in cells transfected with siCtrl or siSRC siRNAs that were either left untreated or treated with 50 μM Etoposide for 48 h. Representative Western blots are in **Supplementary Fig. 5h**. **c** Quantification of *PUMA* and *BCL2L2* mRNAs by RT-qPCR analysis (see also **Supplementary Fig. 5i**). Data were normalized to the levels of *ACTB* mRNA. **d** Representative Western blot analysis of the levels of proteins expressed from the transcripts in (c). **e** Levels of phosphorylated SRC (Y418), total SRC, MYC-tag, phospho-p38 (T180/Y182), p38, and p53 in the different conditions tested. The levels of ACTB were assessed to evaluate loading differences. Values indicate the means ± SD from signals obtained in 3 independent experiments. **f** Quantification of *PUMA* and *BCL2L2* mRNAs by RT-qPCR analysis; data were normalized to the levels of *ACTB* mRNA. **g** Representative Western blot analysis of the levels of proteins expressed from the transcripts in (f). **h** Cell viability was assessed in IMR-90 cells

treated with 50 μM Etoposide and either left without further treatment or treated with PP1 or PP2 for 48 h or 10 days. **i** The levels of *PUMA* and *BCL2L2* mRNAs were quantified by RT-qPCR analysis in cells treated with 50 μM etoposide for the times shown; data were normalized to the levels of *ACTB* mRNA. Values shown in b, d-f are means ± SD; significance (*, $P < 0.05$, **, $P < 0.01$, ***, $P < 0.001$) was determined by using two-tailed Student's t-test.

**Figure 6. SRC influence on cell viability via signaling through p38 and p53. a** Percent viable cells present after 48 h of treatment with etoposide (50 μM) plus either vehicle alone or p38i (AL 8697, 10 μM), p53a (Nutlin-3a, 10 μM), p53a+p38i, PP1, or PP2. See also **Supplementary Fig. 6b**. **b** Measurement of the levels of *PUMA* and *BCL2L2* mRNAs by RT-qPCR analysis in cells treated as in (a); data were normalized to *ACTB* mRNA levels. **c** Western blot analysis of the protein levels of PUMA, BCL2L2, p-HSP27 (Ser82), and p53, including ACTB as normalization control. **d** Viability measured by direct cell counting in 200 μM etoposide-treated cells. In transduced cells, expression of the doxycycline-inducible CA-SRC construct (by addition of 1 μg/ml Doxycycline) was triggered simultaneously with the rest of the treatments. **e** Measurement of the levels of *PUMA* and *BCL2L2* mRNAs by RT-qPCR analysis in cells treated as in (d); data are normalized to *ACTB* mRNA levels. **f** Schematic representation of the model described in this study. Senescence-causing DNA damage (*bottom*) enhances SRC activation, leading to decreased p53 function and increased p38 function; it prevents apoptosis by affecting the relative abundance of PUMA and BCL2L2. Apoptosis-causing DNA damage does not activate SRC, and thus cannot establish the survival program mediated by p53 and p38. Statistical analyses were done by using two-tailed Student's t-test. Values shown in a-d are the means ± SD of at least three replicates; significance (*, $P < 0.05$, **, $P < 0.01$, ***, $P < 0.001$) was determined by using two-tailed Student's t-test.

**Figure 7. SRC inhibition prevents accumulation of senescent cells in chemotherapy-induced senescence in mice. a** Overview of the schedule of experiments performed in mice. **b** Viability of IMR-90 fibroblasts treated with senescence-inducing doxorubicin doses (250 nM) plus either vehicle, PP1, or PP2, as measured by direct cell counting 48 hours later. **c** Measurement of the levels of *p21* and *Il6* mRNAs by RT-qPCR analysis in lungs treated as in (a); data were normalized to *Actb* mRNA levels. **d** Representative micrographs of p21 immunofluorescent staining of the experimental groups indicated. Scale bar, 50 μm. **e** Quantification of p21-positive cells in each tissue assayed. See also **Supplementary Fig. 7c,d**. **f** Percentages of TUNEL-positive cells in lungs from the indicated experimental groups. See also **Supplementary Fig. 7e**. Graph in b shows the mean values ± SD of n=3 independent experiments. Graphs in c, e, and f display the means (bars) and each individual value as a dot ± SD of n=6 mice; significance (*, $P < 0.05$, **, $P < 0.01$, ***, $P < 0.001$) was determined by using two-tailed Student's t-test.

Anerillas et al. Figure 1

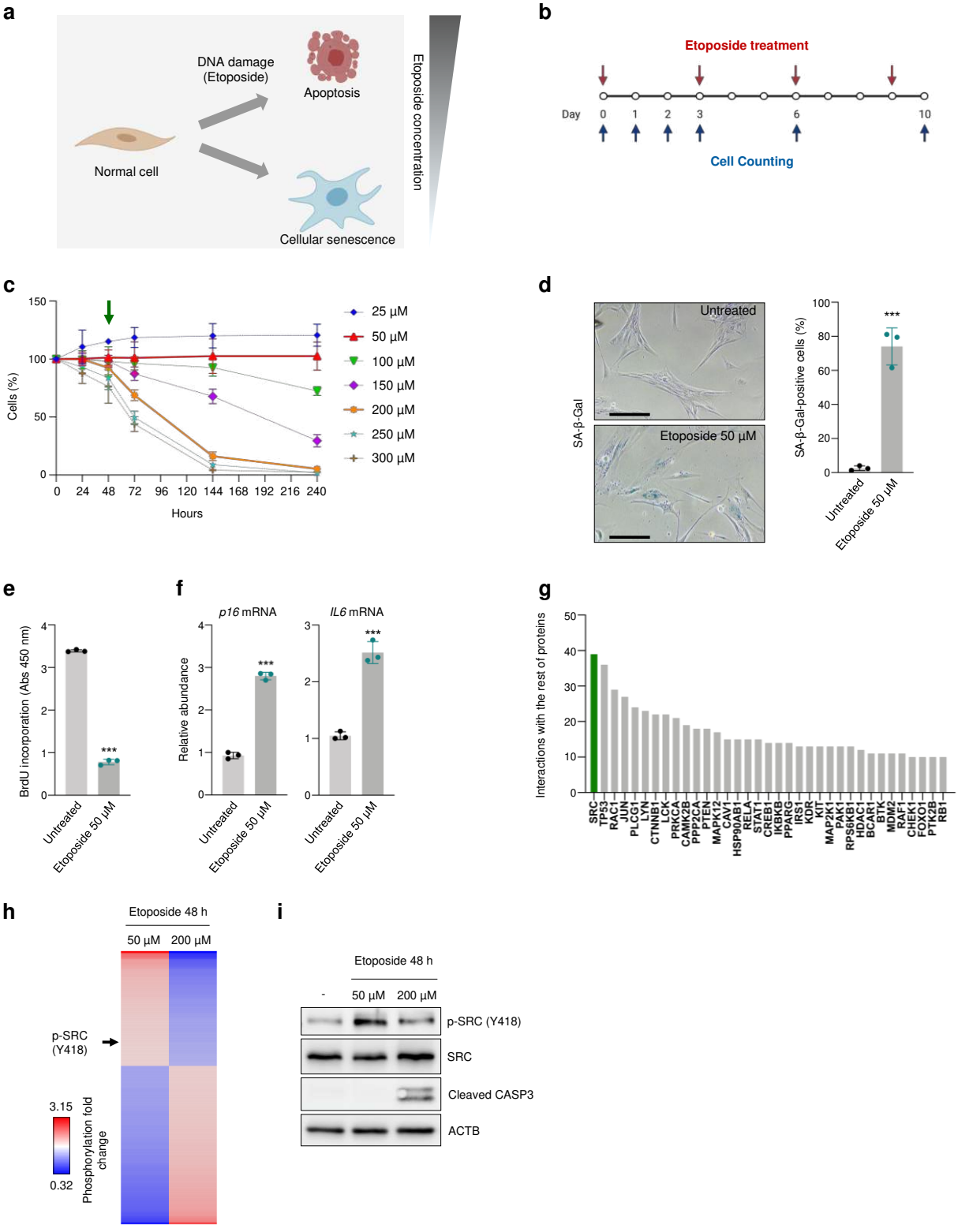


**Figure 1. Pro-survival signaling in senescence-committed cells implicate the SRC pathway. a** Schematic representation of the experimental strategy used to determine the threshold of etoposide required to induce senescence or apoptosis. **b** Timeline of etoposide treatment of proliferating IMR-90 fibroblasts. **c** Percentage of live cells, as assessed by direct cell counts, following etoposide treatment as explained in (b); green arrow indicates the time point selected for subsequent experiments. **d** Representative micrographs of SA-β-gal staining of cells 10 days after either no treatment or treatment with 50 µM etoposide. Scale bar, 100 µm. *Right*, Quantification of the percentage of SA-β-gal-positive

cells in each condition. **e** Measurement of BrdU incorporation in cells that were either left untreated or treated for 10 days with 50 μM etoposide as explained in (B). **f** RT-qPCR assessment of the levels of *p16* and *IL6* mRNAs in cells that were either untreated or treated for 10 days with 50 μM etoposide as explained in (B); data were normalized to *ACTB* mRNA levels. **g** STRING analysis of proteins differentially phosphorylated 48 h after treating cells with 50 or 200 μM etoposide. The graph represents the number of protein interactions identified for the indicated protein. **h** Heat map representation of the protein sites with significantly changed phosphorylation status between 50 and 200 μM etoposide treatment (see also **Supplementary Fig. 1**; data are means of n=2 per condition). Arrow indicates SRC phosphorylated at Y418. *Left*, color representation of fold changes. **i** Representative Western blot analysis of Phospho-SRC (Y418), total SRC, cleaved Caspase3 (CASP3), and loading control β-Actin (ACTB) of whole-cell lysates from IMR-90 cultures that were either left untreated or treated with 50 or 200 μM etoposide. Graphs in **c-f** display the mean values ± SD of n=3 experiments; significance (*, $P < 0.05$, **, $P < 0.01$, ***, $P < 0.001$) was determined by using two-tailed Student's t-test.

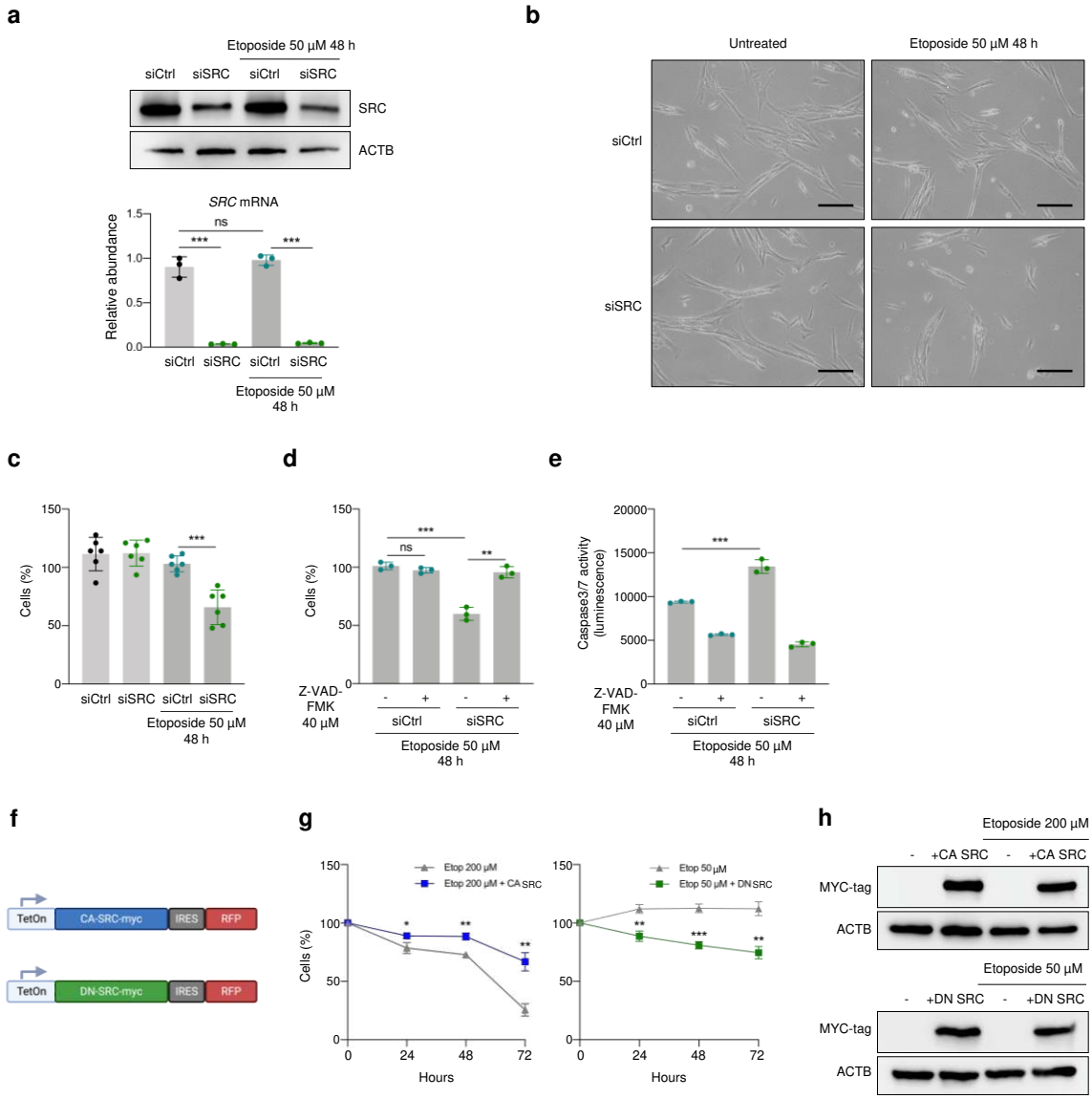


**Figure 2. Modulation of SRC activity in IMR-90 cells controls cell fate after etoposide treatment.** **a** Levels of SRC protein, as assessed by Western blot analysis (top) and *SRC* mRNA, as assessed by RT-qPCR analysis (bottom) in IMR-90 fibroblasts that were either left untreated or treated for 48 h with 50 µM etoposide. **b** Representative micrographs of IMR-90 fibroblasts transfected with either control siRNA (siCtrl) or siRNA directed at *SRC* mRNA (siSRC), and were either left untreated or treated with etoposide 50 µM for 48 h. **c** Cells were treated as described in (B); live cells were counted after 48 hours. **d, e** Cells were transfected with the siRNAs shown; 48 h later they were either left untreated or treated with the Caspase inhibitor Z-VAD-FMK in the presence of 50 µM etoposide; 48 h later, cell viability was assessed by direct cell counting of remaining cells (d), and Caspase 3/7-dependent luciferase activity was assessed in each group (e). **f-h** Schematic representation of the constitutively active (CA) and dominant-negative (DN) SRC lentiviral constructs generated (f). IMR-90 cells were transduced with CA-SRC or DN-SRC (g) and induced by doxycycline (1 µg/ml) in cells treated with either 200 µM or 50 µM (g) etoposide. Cell viability was monitored by direct cell counting and plotted as a percentage of cells at time 0. Western blot analysis of the levels of MYC-tagged SRC mutants (see also **Supplementary Fig. 3a**) after 72 h in the presence of doxycycline; ACTB was included as a loading control (h). Graphs in a, c-e, g represent the mean values ± SD of n=3 experiments; significance (*, $P < 0.05$, **, $P < 0.01$, ***, $P < 0.001$) was determined by using two-tailed Student's t-test.

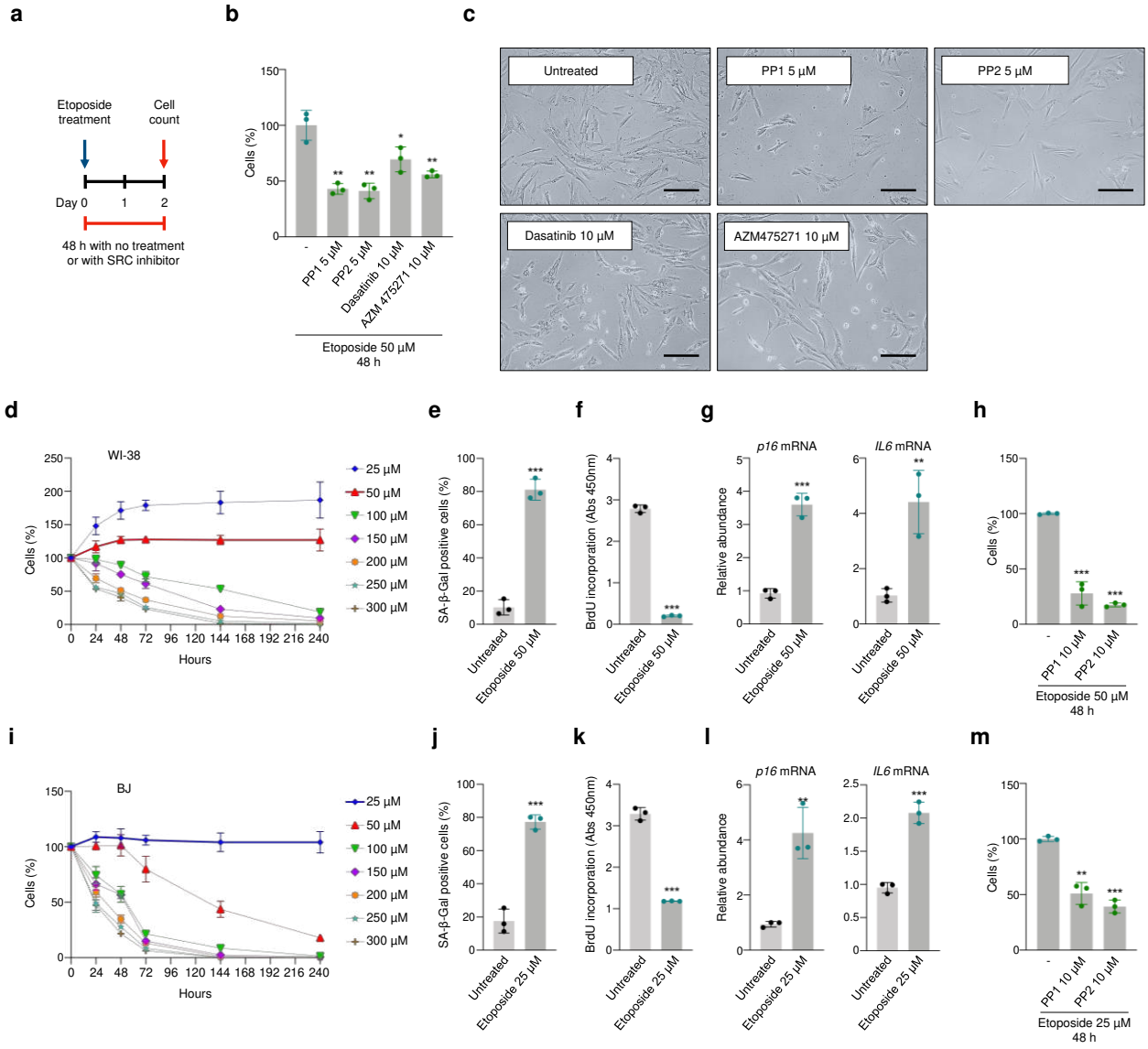


**Figure 3. Inhibition of SRC kinase activity skews towards apoptosis instead of senescence.** **a** Schematic describing the schedule of treatments with SRC inhibitor and etoposide. **b** Cell viability was measured by direct cell counting 48 h after simultaneous treatment of IMR-90 cells with 50 µM etoposide and either no further treatment or treatment with SRC inhibitors. **c** Representative micrographs 48 h after simultaneous treatment of IMR-90 fibroblasts with 50 µM etoposide and the indicated SRC inhibitors. Scale bars, 100 µm. **d** Cell viability was assessed in each treatment group by direct counting of WI-38 cells at the times and etoposide concentrations shown. **e-g** Cellular senescence at day 10 was assessed by SA-β-gal staining (e), BrdU incorporation (f), and RT-qPCR analysis of the levels of senescence markers *p16* and *IL6* mRNA, normalized to the levels of *ACTB* mRNA (g). **h** Viability was determined by direct counting of human WI-38 fibroblasts treated with 50 µM etoposide in the absence or presence PP1 or PP2. **i** Percentages of live cells as assessed by direct counting of human BJ fibroblasts treated with different etoposide doses. **j-l** Assessment of senescence in BJ fibroblasts at day 10 of treatment with 25 µM etoposide by SA-β-gal staining (j), BrdU incorporation (k), and RT-qPCR assessment of the levels of *p16* and *IL6* mRNAs (l). **m** Cell viability after joint treatment with 25 µM etoposide and PP1 or PP2 as described for IMR-90 cells (a) and WI-38 cells (b, h). In panels (b, d, f, g, i, j), significance was assessed by two-tailed Student's t-test. Graphs represent the mean values ± SD of n=3 experiments; significance (*, $P < 0.05$, **, $P < 0.01$, ***, $P < 0.001$) was determined by using two-tailed Student's t-test.

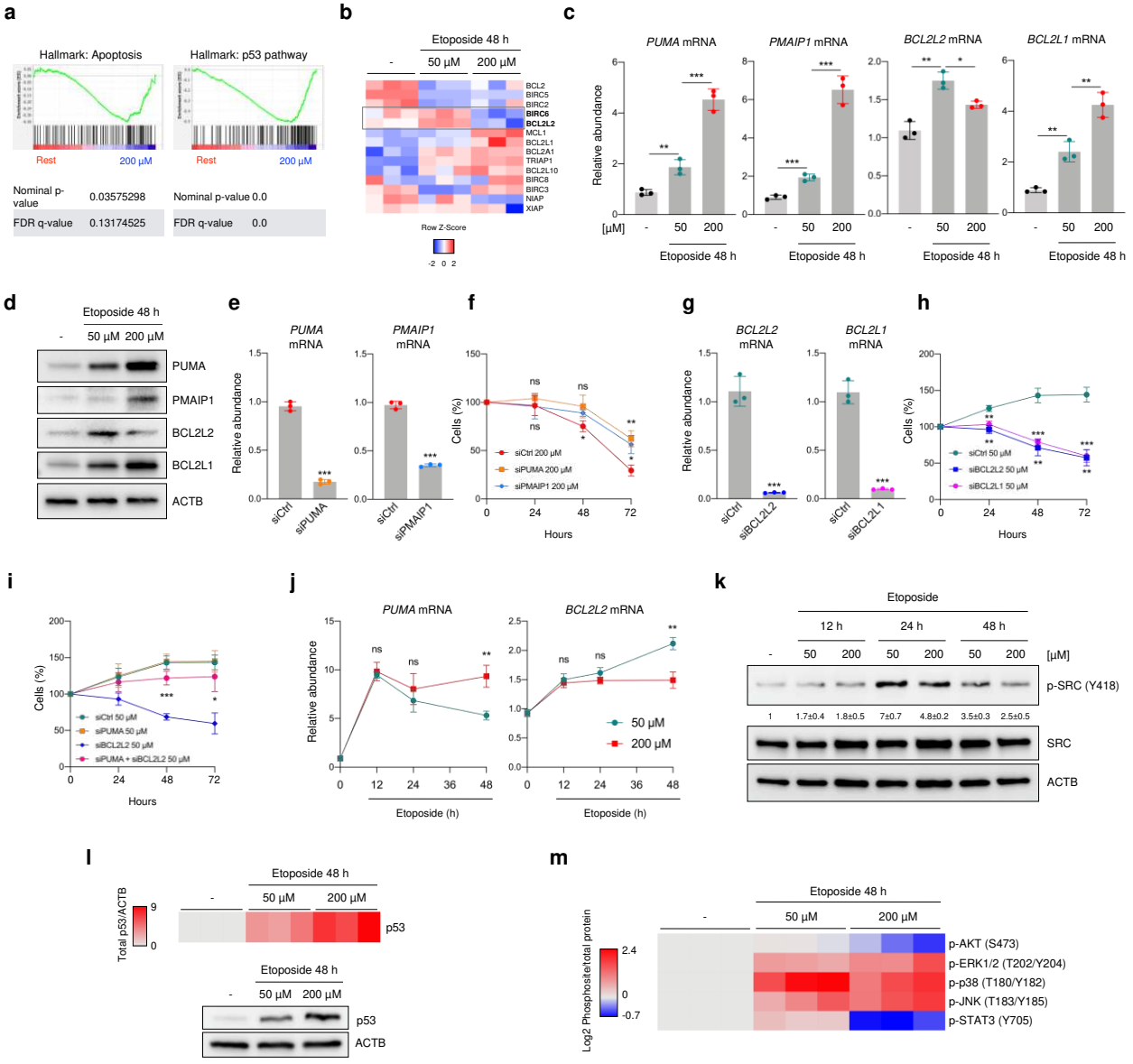


**Figure 4. Essential genes for cell fate determination are regulated by signaling through SRC. a, b** GSEA analysis plots (a) and heat map (b) depicting transcriptomic (microarray) analysis of mRNAs encoding pro-apoptotic (a) or pro-survival (b) proteins in cells that were either left untreated (-) or treated for 48 h with 50 or 200 μM etoposide. Data shown in (b) are raw Z Score of the Log2-normalized expression values for each transcript (n=3 per condition). **c** Validation of the top microarray target transcripts, *PUMA, PMAIP1, BCL2L2*, and *BCL2L1* mRNAs by RT-qPCR analysis (see also **Supplementary Fig. 5a**). **d** Representative Western blot analysis of the levels of PUMA, PMAIP1, BCL2L2, and BCL2L1 proteins in cells treated as indicated in (a). **e** RT-qPCR assessment of the levels of *PUMA* and *PMAIP1* mRNAs 72 h after transfection with specific siRNAs (normalized to *ACTB* mRNA levels). **f** Cells were transfected with either siCtrl, siPUMA, or siPMAIP1 siRNAs and treated with 200 μM etoposide; cell viability was assessed by direct cell counting at the times indicated (see also **Supplementary Fig. 5b**). Significant differences are indicated above the curves (siPUMA vs siCtrl), and below the curves (siPMAIP1 vs siCtrl). **g** RT-qPCR assessment of the levels of *BCL2L2* and *BCL2L1* mRNAs 72 h after transfection with specific siRNAs (normalized to *ACTB* mRNA levels). **h** Cells were transfected with either siCtrl, siBCL2L2, or siBCL2L1 siRNAs and treated with 50 μM etoposide; cell viability was assessed by direct cell counting at the indicated times (see also

**Supplementary Fig. 5e**). Significant differences are indicated above the curves (siBCL2L1 vs siCtrl), and below the curves (siBCL2L2 vs siCtrl). **i** Cells were transfected with either siCtrl, siPUMA, siBCL2L2, or siPUMA+siBCL2L2 siRNAs and treated with 50 μM etoposide; cell viability was assessed by direct cell counting at the indicated times (see also **Supplementary Fig. 5e**). Significant differences are indicated. **j** Influence of etoposide (50 or 200 μM) on the time-dependent abundance of *PUMA* and *BCL2L2* mRNAs, as assessed by RT-qPCR analysis (normalized to *ACTB* mRNA levels). **k** Representative Western blot analysis of the levels of SRC, phosphorylated SRC (Y418), and loading control ACTB in IMR-90 cells treated with 50 or 200 μM etoposide for the times indicated. Values below the blot represent the means ± SD from densitometric quantification of signals in n=3 experiments. **l** Heat map representation (*top*) of quantified densitometry signals from p53 by Western blot analysis (bottom) in IMR-90 cells that were either left untreated or treated with 50 μM or 200 μM etoposide for 48 hours. **m** Heat map representation of the quantified densitometry signals on western blots detecting phosphorylated protein relative to corresponding total protein. Representative Western blots are in **Supplementary Fig. 5g**. Data are represented as Log2 of the normalized values. Graphs (c, e-j) represent the means ± SD from n=3 experiments; significance (*, $P < 0.05$, **, $P < 0.01$, ***, $P < 0.001$) was determined by using two-tailed Student's t-test.

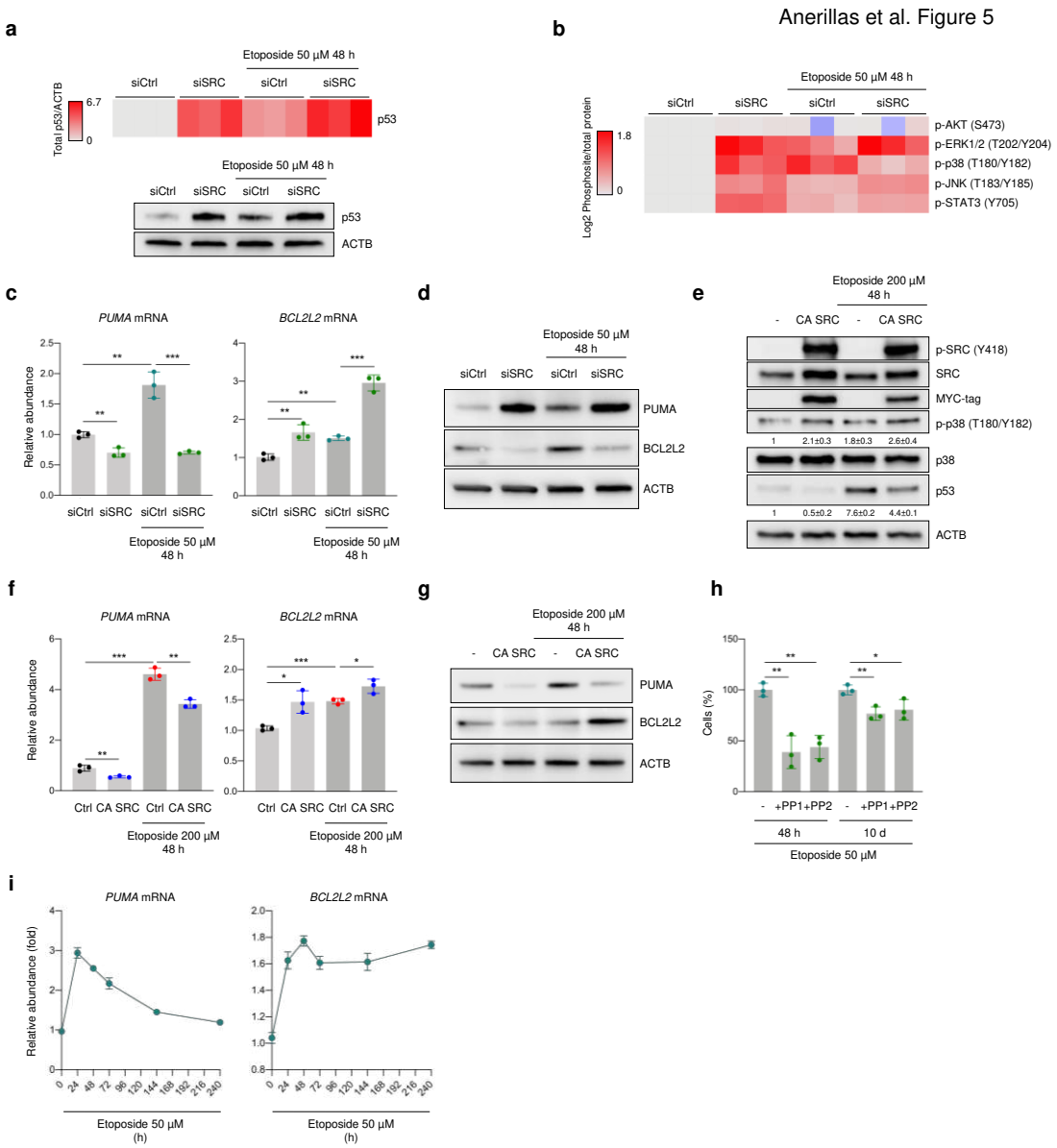


**Figure 5. SRC represses p53 and promotes p38 signaling to favor survival in early senescence.** **a** Heat map representation of p53 levels (*top*) quantified by densitometry from signals on western blots (*bottom*, representative panel) in IMR-90 cells transfected with siCtrl or siSRC siRNAs, either untreated or treated with 50 µM Etoposide for 48 h. **b** Heat map representation of densitometry quantification of signals on western blots detecting phosphorylated residues, normalized to protein levels assessed in cells transfected with siCtrl or siSRC siRNAs that were either left untreated or treated with 50 µM Etoposide for 48 h. Representative Western blots are in **Supplementary Fig. 5h**. **c** Quantification of *PUMA* and *BCL2L2* mRNAs by RT-qPCR analysis (see also **Supplementary Fig. 5i**). Data were normalized to the levels of *ACTB* mRNA. **d** Representative Western blot analysis of the levels of proteins expressed from the transcripts in (c). **e** Levels of phosphorylated SRC (Y418), total SRC, MYC-tag, phospho-p38 (T180/Y182), p38, and p53 in the different conditions tested. The levels of ACTB were assessed to evaluate loading differences. Values indicate the means ± SD from signals obtained in 3 independent experiments. **f** Quantification of *PUMA* and *BCL2L2* mRNAs by RT-qPCR analysis; data were normalized to the levels of *ACTB* mRNA. **g** Representative Western blot analysis of the levels of proteins expressed from the transcripts in (f). **h** Cell viability was assessed in IMR-90 cells treated with 50 µM Etoposide and either left without further treatment or treated with PP1 or PP2 for 48 h or 10 days. **i** The levels of *PUMA* and *BCL2L2* mRNAs were quantified by RT-qPCR analysis in cells treated with 50 µM etoposide for the times shown; data were normalized to the levels of *ACTB* mRNA. Values shown in b, d-f are means ± SD; significance (*, $P < 0.05$, **, $P < 0.01$, ***, $P < 0.001$) was determined by using two-tailed Student's t-test.

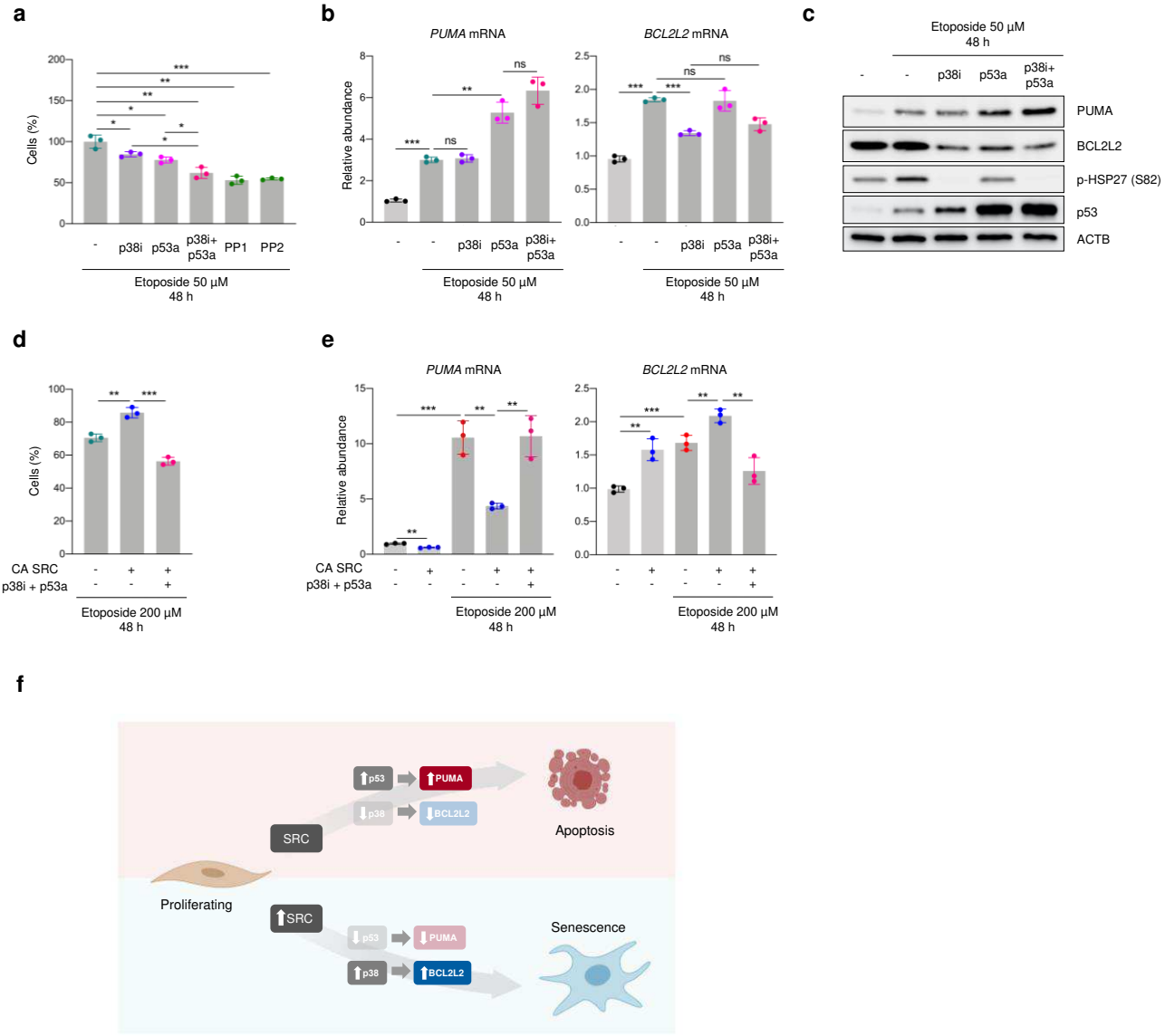


**Figure 6. SRC influence on cell viability via signaling through p38 and p53.** **a** Percent viable cells present after 48 h of treatment with etoposide (50 µM) plus either vehicle alone or p38i (AL 8697, 10 µM), p53a (Nutlin-3a, 10 µM), p53a+p38i, PP1, or PP2. See also **Supplementary Fig. 6b**. **b** Measurement of the levels of *PUMA* and *BCL2L2* mRNAs by RT-qPCR analysis in cells treated as in (a); data were normalized to *ACTB* mRNA levels. **c** Western blot analysis of the protein levels of PUMA, BCL2L2, p-HSP27 (Ser82), and p53, including ACTB as normalization control. **d** Viability measured by direct cell counting in 200 µM etoposide-treated cells. In transduced cells, expression of the doxycycline-inducible CA-SRC construct (by addition of 1 µg/ml Doxycycline) was triggered simultaneously with the rest of the treatments. **e** Measurement of the levels of *PUMA* and *BCL2L2* mRNAs by RT-qPCR analysis in cells treated as in (d); data are normalized to *ACTB* mRNA levels. **f** Schematic representation of the model described in this study. Senescence-causing DNA damage (*bottom*) enhances SRC activation, leading to decreased p53 function and increased p38 function; it prevents apoptosis by affecting the relative abundance of PUMA and BCL2L2. Apoptosis-causing DNA damage does not activate SRC, and thus cannot establish the survival program mediated by p53 and p38. Statistical analyses were done by using two-tailed Student's t-test. Values shown in a-d are the means ± SD of at least three replicates; significance (*, $P < 0.05$, **, $P < 0.01$, ***, $P < 0.001$) was determined by using two-tailed Student's t-test.

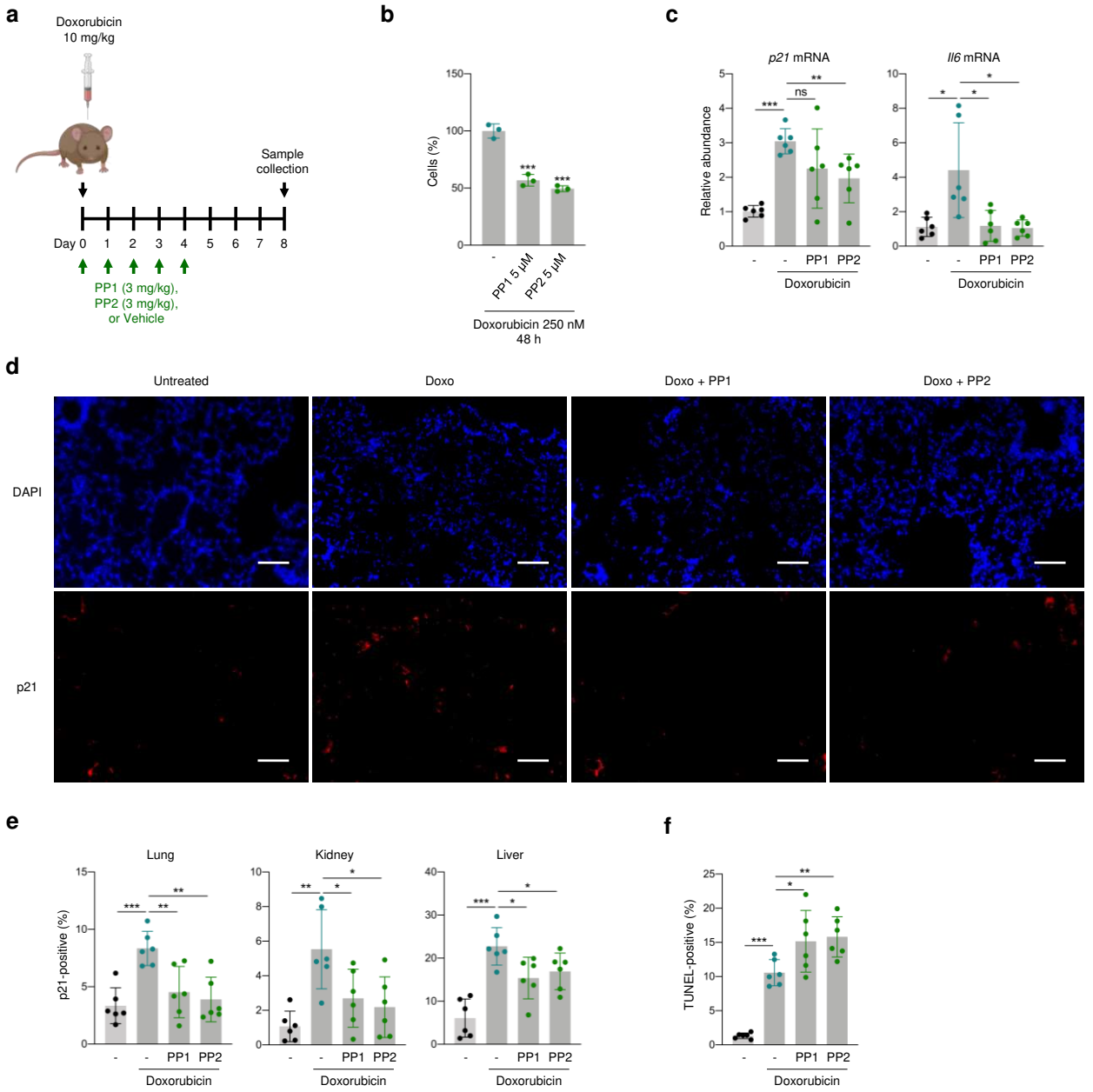


**Figure 7. SRC inhibition prevents accumulation of senescent cells in chemotherapy-induced senescence in mice.** **a** Overview of the schedule of experiments performed in mice. **b** Viability of IMR-90 fibroblasts treated with senescence-inducing doxorubicin doses (250 nM) plus either vehicle, PP1, or PP2, as measured by direct cell counting 48 hours later. **c** Measurement of the levels of *p21* and *Il6* mRNAs by RT-qPCR analysis in lungs treated as in (a); data were normalized to *Actb* mRNA levels. **d** Representative micrographs of p21 immunofluorescent staining of the experimental groups indicated. Scale bar, 50 µm. **e** Quantification of p21-positive cells in each tissue assayed. See also **Supplementary Fig. 7c,d**. **f** Percentages of TUNEL-positive cells in lungs from the indicated experimental groups. See also **Supplementary Fig. 7e**. Graph in b shows the mean values ± SD of n=3 independent experiments. Graphs in c, e, and f display the means (bars) and each individual value as a dot ± SD of n=6 mice; significance (*, $P < 0.05$, **, $P < 0.01$, ***, $P < 0.001$) was determined by using two-tailed Student's t-test.

# Figures

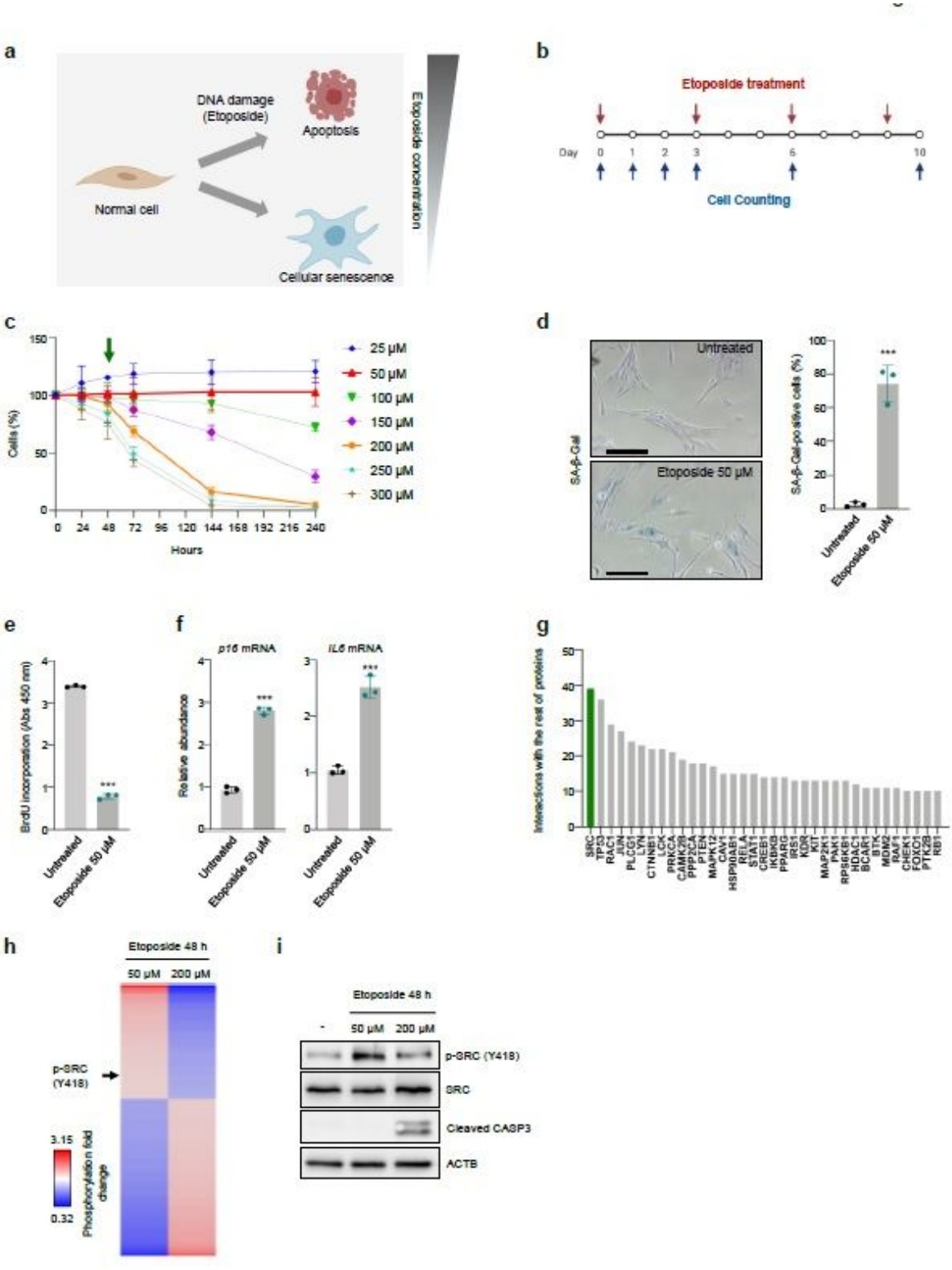


**Figure 1**

Pro-survival signaling in senescence-committed cells implicate the SRC pathway. a Schematic representation of the experimental strategy used to determine the threshold of etoposide required to induce senescence or apoptosis. b Timeline of etoposide treatment of proliferating IMR-90 fibroblasts. c

Percentage of live cells, as assessed by direct cell counts, following etoposide treatment as explained in (b); green arrow indicates the time point selected for subsequent experiments. d Representative micrographs of SA-β-gal staining of cells 10 days after either no treatment or treatment with 50 μM etoposide. Scale bar, 100 μm. Right, Quantification of the percentage of SA-β-gal-positive cells in each condition. e Measurement of BrdU incorporation in cells that were either left untreated or treated for 10 days with 50 μM etoposide as explained in (B). f RT-qPCR assessment of the levels of p16 and IL6 mRNAs in cells that were either untreated or treated for 10 days with 50 μM etoposide as explained in (B); data were normalized to ACTB mRNA levels. g STRING analysis of proteins differentially phosphorylated 48 h after treating cells with 50 or 200 μM etoposide. The graph represents the number of protein interactions identified for the indicated protein. h Heat map representation of the protein sites with significantly changed phosphorylation status between 50 and 200 μM etoposide treatment (see also Supplementary Fig. 1; data are means of n=2 per condition). Arrow indicates SRC phosphorylated at Y418. Left, color representation of fold changes. i Representative Western blot analysis of Phospho-SRC (Y418), total SRC, cleaved Caspase3 (CASP3), and loading control β-Actin (ACTB) of whole-cell lysates from IMR-90 cultures that were either left untreated or treated with 50 or 200 μM etoposide. Graphs in c-f display the mean values ± SD of n=3 experiments; significance (*, $P < 0.05$, **, $P < 0.01$, ***, $P < 0.001$) was determined by using two-tailed Student's t-test.

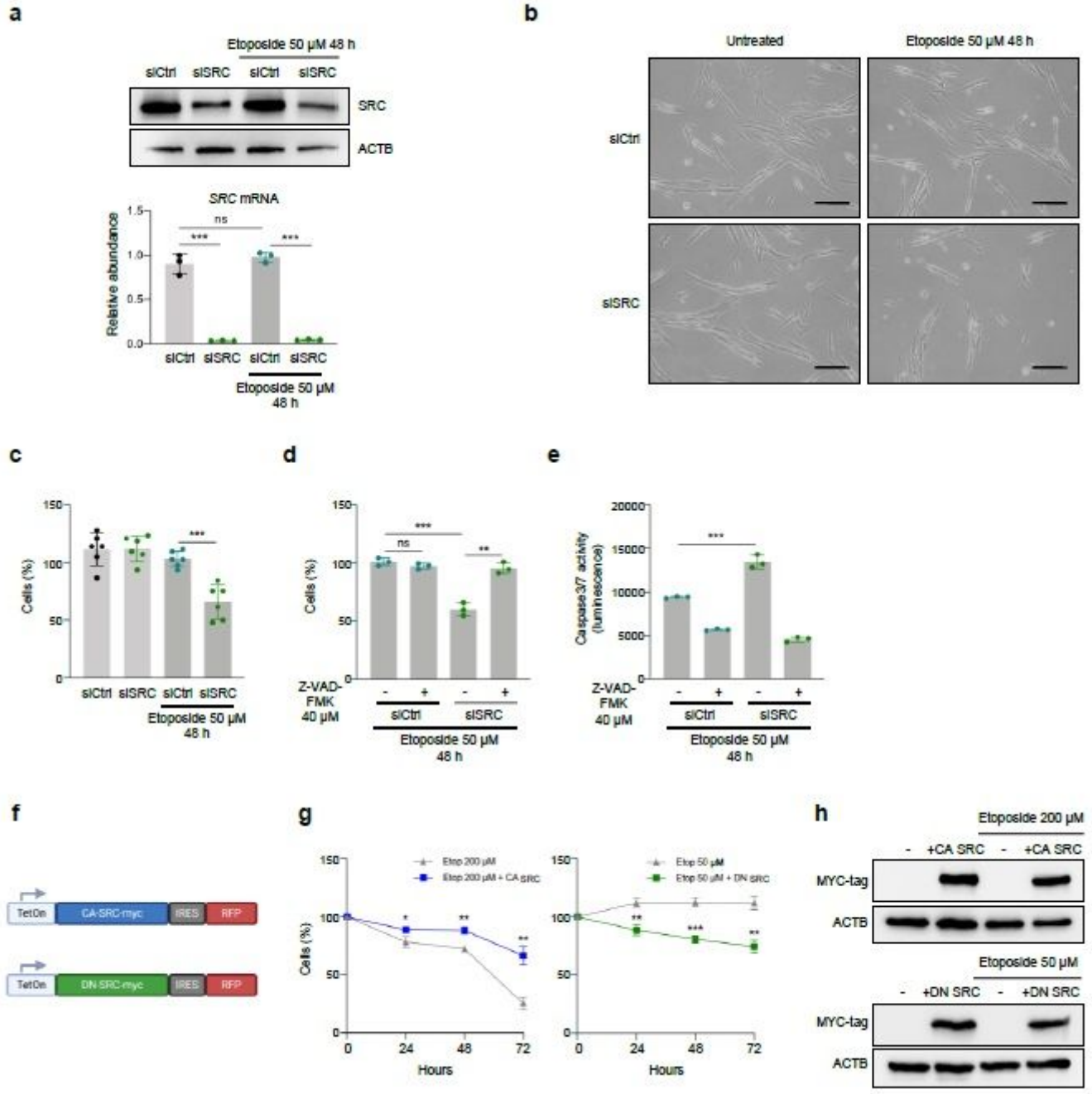


## Figure 2

Modulation of SRC activity in IMR-90 cells controls cell fate after etoposide treatment. a Levels of SRC protein, as assessed by Western blot analysis (top) and SRC mRNA, as assessed by RT-qPCR analysis (bottom) in IMR-90 fibroblasts that were either left untreated or treated for 48 h with 50 µM etoposide. b Representative micrographs of IMR-90 fibroblasts transfected with either control siRNA (siCtrl) or siRNA directed at SRC mRNA (siSRC), and were either left untreated or treated with etoposide 50 µM for 48 h. c Cells were treated as described in (B); live cells were counted after 48 hours. d, e Cells were transfected with the siRNAs shown; 48 h later they were either left untreated or treated with the Caspase inhibitor Z-VAD-FMK in the presence of 50 µM etoposide; 48 h later, cell viability was assessed by direct cell counting of remaining cells (d), and Caspase 3/7-dependent luciferase activity was assessed in each group (e). f-h

Schematic representation of the constitutively active (CA) and dominant-negative (DN) SRC lentiviral constructs generated (f). IMR-90 cells were transduced with CA-SRC or DN-SRC (g) and induced by doxycycline (1 µg/ml) in cells treated with either 200 µM or 50 µM (g) etoposide. Cell viability was monitored by direct cell counting and plotted Anerillas et al., page as a percentage of cells at time 0. Western blot analysis of the levels of MYC-tagged SRC mutants (see also Supplementary Fig. 3a) after 72 h in the presence of doxycycline; ACTB was included as a loading control (h). Graphs in a, c-e, g represent the mean values ± SD of n=3 experiments; significance (*, P < 0.05, **, P < 0.01, ***, P < 0.001) was determined by using two-tailed Student's t-test.

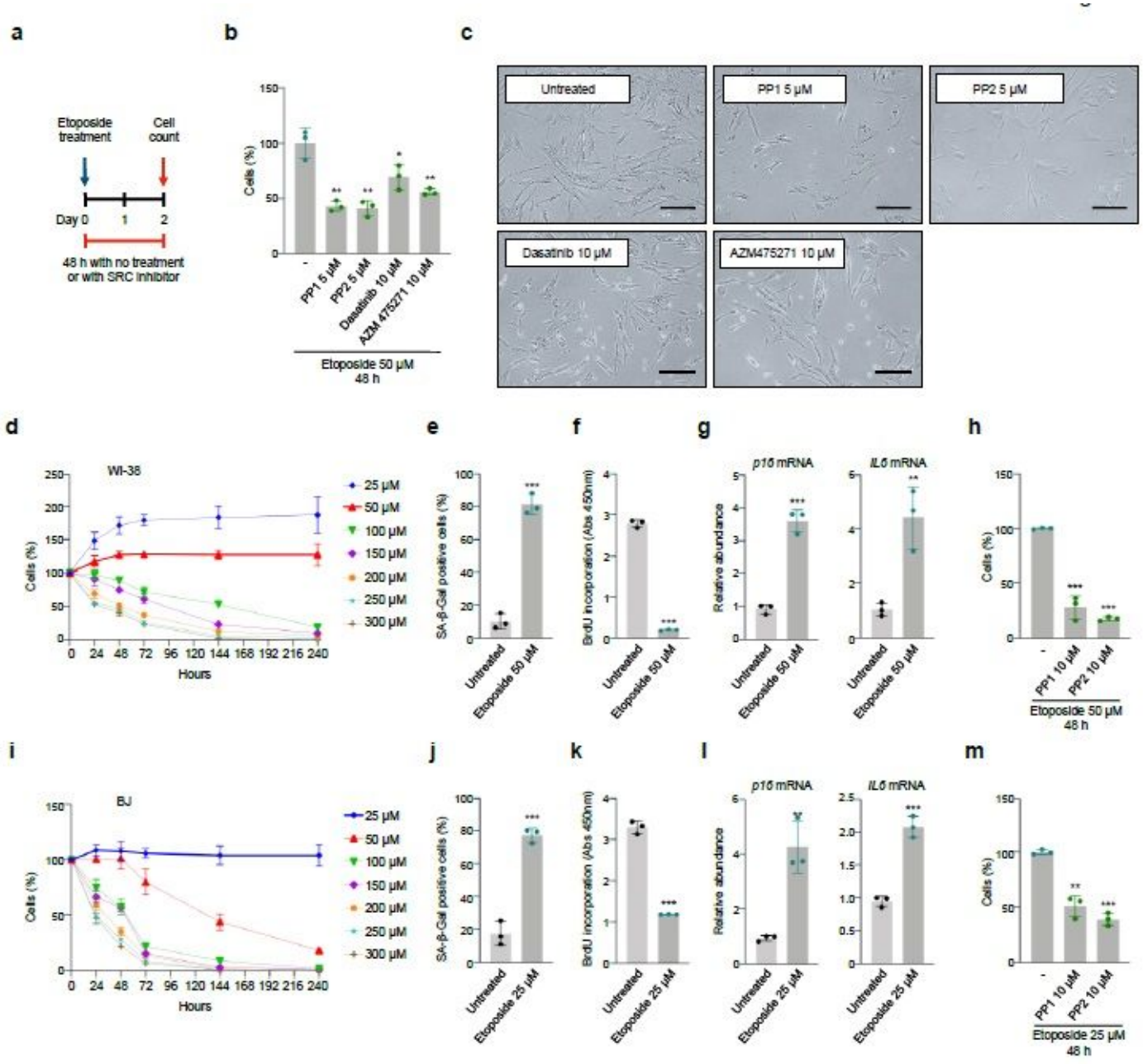


## Figure 3

Inhibition of SRC kinase activity skews towards apoptosis instead of senescence. a Schematic describing the schedule of treatments with SRC inhibitor and etoposide. b Cell viability was measured by direct cell

counting 48 h after simultaneous treatment of IMR-90 cells with 50 μM etoposide and either no further treatment or treatment with SRC inhibitors. c Representative micrographs 48 h after simultaneous treatment of IMR-90 fibroblasts with 50 μM etoposide and the indicated SRC inhibitors. Scale bars, 100 μm. d Cell viability was assessed in each treatment group by direct counting of WI-38 cells at the times and etoposide concentrations shown. e-g Cellular senescence at day 10 was assessed by SA-β-gal staining (e), BrdU incorporation (f), and RT-qPCR analysis of the levels of senescence markers p16 and IL6 mRNA, normalized to the levels of ACTB mRNA (g). h Viability was determined by direct counting of human WI-38 fibroblasts treated with 50 μM etoposide in the absence or presence PP1 or PP2. i Percentages of live cells as assessed by direct counting of human BJ fibroblasts treated with different etoposide doses. j-l Assessment of senescence in BJ fibroblasts at day 10 of treatment with 25 μM etoposide by SA-β-gal staining (j), BrdU incorporation (k), and RT-qPCR assessment of the levels of p16 and IL6 mRNAs (l). m Cell viability after joint treatment with 25 μM etoposide and PP1 or PP2 as described for IMR-90 cells (a) and WI-38 cells (b, h). In panels (b, d, f, g, i, j), significance was assessed by two-tailed Student's t-test. Graphs represent the mean values ± SD of n=3 experiments; significance (*, $P < 0.05$, **, $P < 0.01$, ***, $P < 0.001$) was determined by using two-tailed Student's t-test.

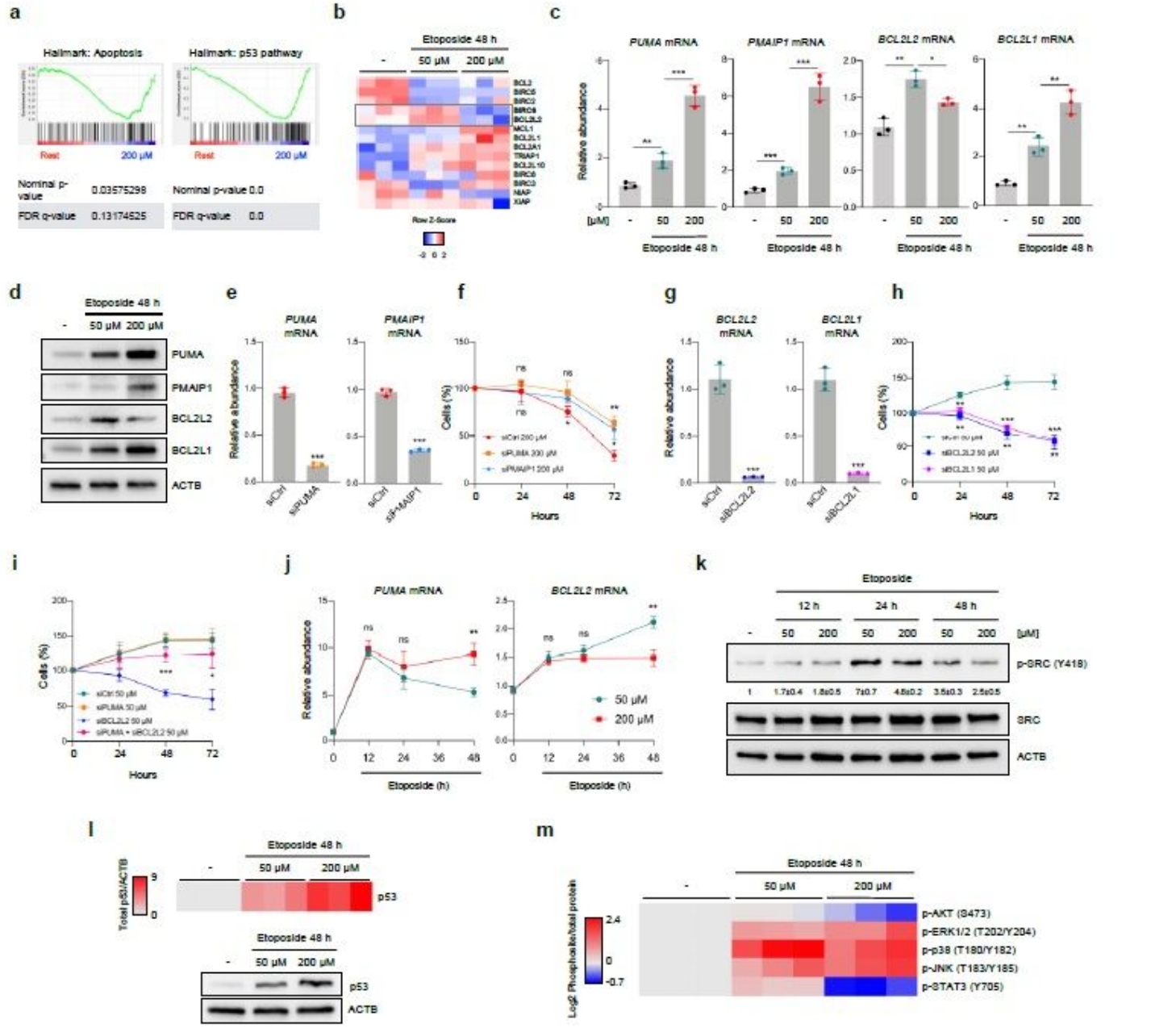


## Figure 4

Essential genes for cell fate determination are regulated by signaling through SRC. a, b GSEA analysis plots (a) and heat map (b) depicting transcriptomic (microarray) analysis of mRNAs encoding pro-apoptotic (a) or pro-survival (b) proteins in cells that were either left untreated (-) or treated for 48 h with 50 or 200 µM etoposide. Data shown in (b) are raw Z Score of the Log2-normalized expression values for each transcript (n=3 per condition). c Validation of the top microarray target transcripts, PUMA, PMAIP1, BCL2L2, and BCL2L1 mRNAs by RT-qPCR analysis (see also Supplementary Fig. 5a). d Representative Western blot analysis of the levels of PUMA, PMAIP1, BCL2L2, and BCL2L1 proteins in cells treated as indicated in (a). e RT-qPCR assessment of the levels of PUMA and PMAIP1 mRNAs 72 h after transfection with specific siRNAs (normalized to ACTB mRNA levels). f Cells were transfected with either siCtrl,

siPUMA, or siPMAIP1 siRNAs and treated with 200 μM etoposide; cell viability was assessed by direct cell counting at the times indicated (see also Supplementary Fig. 5b). Significant differences are indicated above the curves (siPUMA vs Anerillas et al., page siCtrl), and below the curves (siPMAIP1 vs siCtrl). g RT-qPCR assessment of the levels of BCL2L2 and BCL2L1 mRNAs 72 h after transfection with specific siRNAs (normalized to ACTB mRNA levels). h Cells were transfected with either siCtrl, siBCL2L2, or siBCL2L1 siRNAs and treated with 50 μM etoposide; cell viability was assessed by direct cell counting at the indicated times (see also Supplementary Fig. 5e). Significant differences are indicated above the curves (siBCL2L1 vs siCtrl), and below the curves (siBCL2L2 vs siCtrl). i Cells were transfected with either siCtrl, siPUMA, siBCL2L2, or siPUMA+siBCL2L2 siRNAs and treated with 50 μM etoposide; cell viability was assessed by direct cell counting at the indicated times (see also Supplementary Fig. 5e). Significant differences are indicated. j Influence of etoposide (50 or 200 μM) on the time-dependent abundance of PUMA and BCL2L2 mRNAs, as assessed by RT-qPCR analysis (normalized to ACTB mRNA levels). k Representative Western blot analysis of the levels of SRC, phosphorylated SRC (Y418), and loading control ACTB in IMR-90 cells treated with 50 or 200 μM etoposide for the times indicated. Values below the blot represent the means ± SD from densitometric quantification of signals in n=3 experiments. l Heat map representation (top) of quantified densitometry signals from p53 by Western blot analysis (bottom) in IMR-90 cells that were either left untreated or treated with 50 μM or 200 μM etoposide for 48 hours. m Heat map representation of the quantified densitometry signals on western blots detecting phosphorylated protein relative to corresponding total protein. Representative Western blots are in Supplementary Fig. 5g. Data are represented as Log2 of the normalized values. Graphs (c, e-j) represent the means ± SD from n=3 experiments; significance (*, $P < 0.05$, **, $P < 0.01$, ***, $P < 0.001$) was determined by using two-tailed Student's t-test.

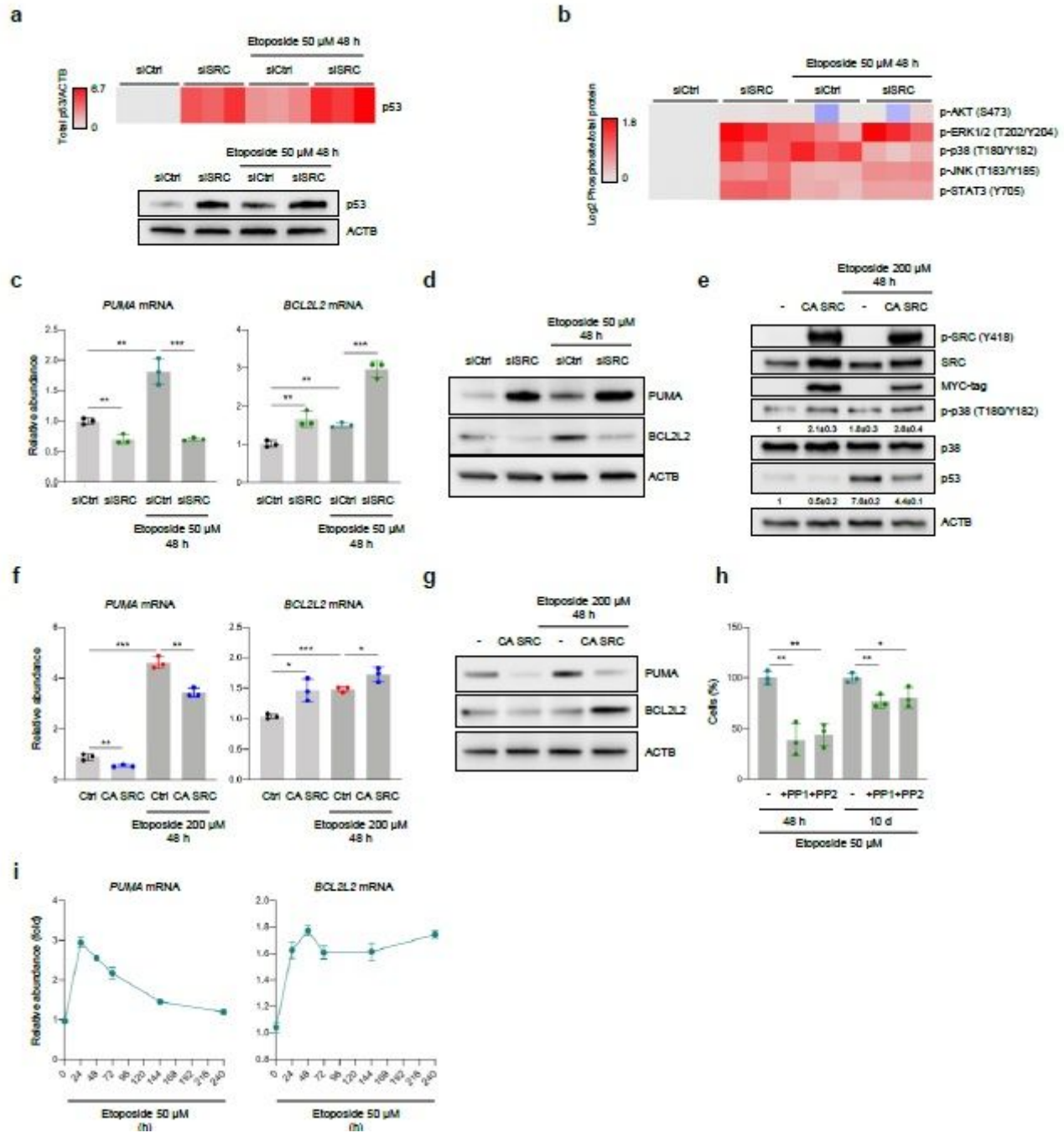


## Figure 5

SRC represses p53 and promotes p38 signaling to favor survival in early senescence. a Heat map representation of p53 levels (top) quantified by densitometry from signals on western blots (bottom, representative panel) in IMR-90 cells transfected with siCtrl or siSRC siRNAs, either untreated or treated with 50 µM Etoposide for 48 h. b Heat map representation of densitometry quantification of signals on western blots detecting phosphorylated residues, normalized to protein levels assessed in cells transfected with siCtrl or siSRC siRNAs that were either left untreated or treated with 50 µM Etoposide for 48 h. Representative Western blots are in Supplementary Fig. 5h. c Quantification of PUMA and BCL2L2 mRNAs by RT-qPCR analysis (see also Supplementary Fig. 5i). Data were normalized to the levels of ACTB mRNA. d Representative Western blot analysis of the levels of proteins expressed from the

transcripts in (c). e Levels of phosphorylated SRC (Y418), total SRC, MYC-tag, phospho-p38 (T180/Y182), p38, and p53 in the different conditions tested. The levels of ACTB were assessed to evaluate loading differences. Values indicate the means ± SD from signals obtained in 3 independent experiments. f Quantification of PUMA and BCL2L2 mRNAs by RT-qPCR analysis; data were normalized to the levels of ACTB mRNA. g Representative Western blot analysis of the levels of proteins expressed from the transcripts in (f). h Cell viability was assessed in IMR-90 cells Anerillas et al., page 27 treated with 50 μM Etoposide and either left without further treatment or treated with PP1 or PP2 for 48 h or 10 days. i The levels of PUMA and BCL2L2 mRNAs were quantified by RT-qPCR analysis in cells treated with 50 μM etoposide for the times shown; data were normalized to the levels of ACTB mRNA. Values shown in b, d-f are means ± SD; significance (*, P < 0.05, **, P < 0.01, ***, P < 0.001) was determined by using two-tailed Student's t-test.

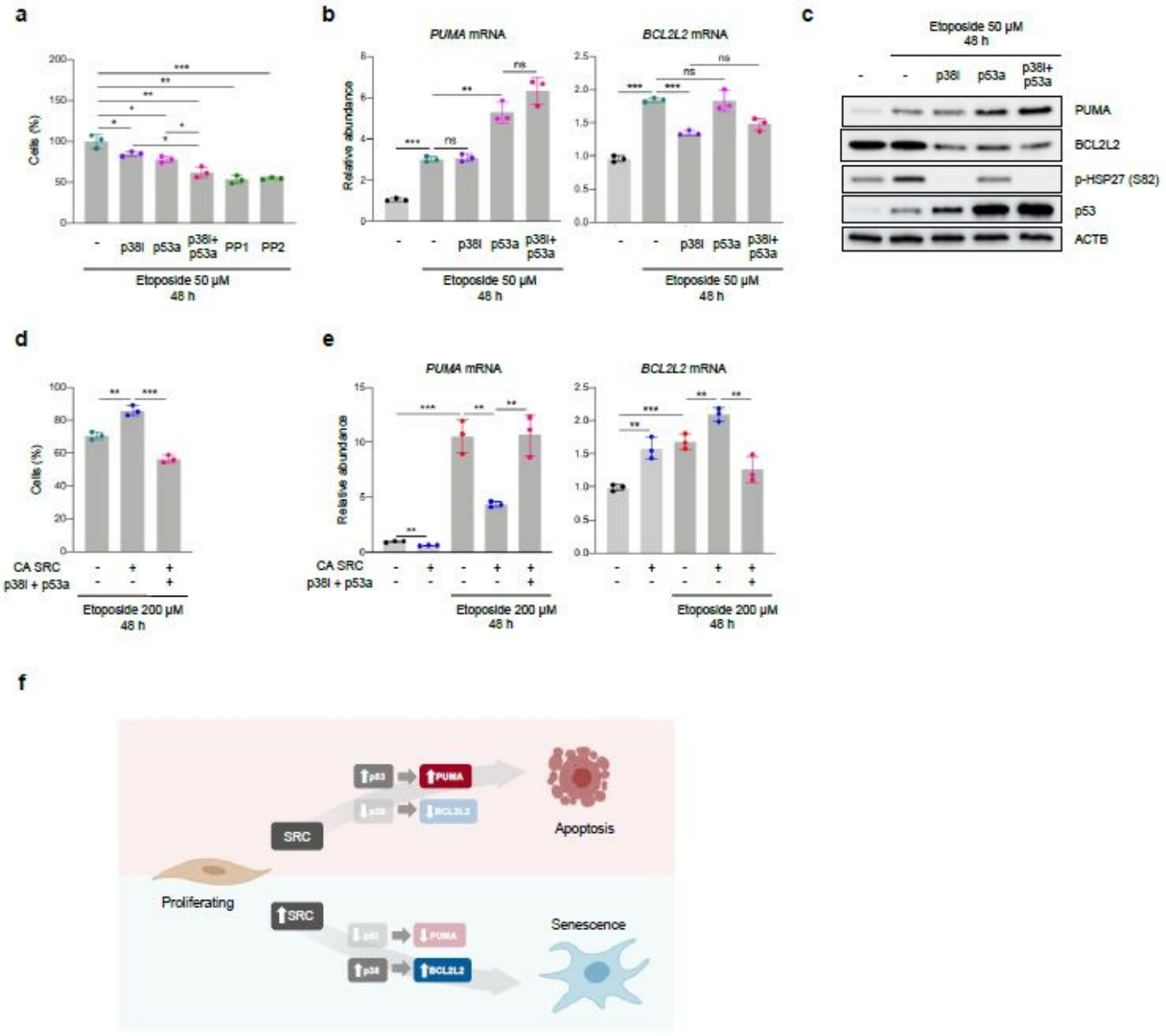


Figure 6

SRC influence on cell viability via signaling through p38 and p53. a Percent viable cells present after 48 h of treatment with etoposide (50 μM) plus either vehicle alone or p38i (AL 8697, 10 μM), p53a (Nutlin-3a, 10 μM), p53a+p38i, PP1, or PP2. See also Supplementary Fig. 6b. b Measurement of the levels of PUMA and BCL2L2 mRNAs by RT-qPCR analysis in cells treated as in (a); data were normalized to ACTB mRNA levels. c Western blot analysis of the protein levels of PUMA, BCL2L2, p-HSP27 (Ser82), and p53, including ACTB as normalization control. d Viability measured by direct cell counting in 200 μM etoposide-treated cells. In transduced cells, expression of the doxycycline-inducible CA-SRC construct (by addition of 1 μg/ml Doxycycline) was triggered simultaneously with the rest of the treatments. e Measurement of the levels of PUMA and BCL2L2 mRNAs by RT-qPCR analysis in cells treated as in (d); data are normalized to ACTB mRNA levels. f Schematic representation of the model described in this study. Senescence-causing DNA damage (bottom) enhances SRC activation, leading to decreased p53 function and increased p38 function; it prevents apoptosis by affecting the relative abundance of PUMA and BCL2L2. Apoptosis-causing DNA damage does not activate SRC, and thus cannot establish the survival program mediated by p53 and p38. Statistical analyses were done by using two-tailed Student's t-test. Values shown in a-d are the means ± SD of at least three replicates; significance (*, $P < 0.05$, **, $P < 0.01$, ***, $P < 0.001$) was determined by using two-tailed Student's t-test.

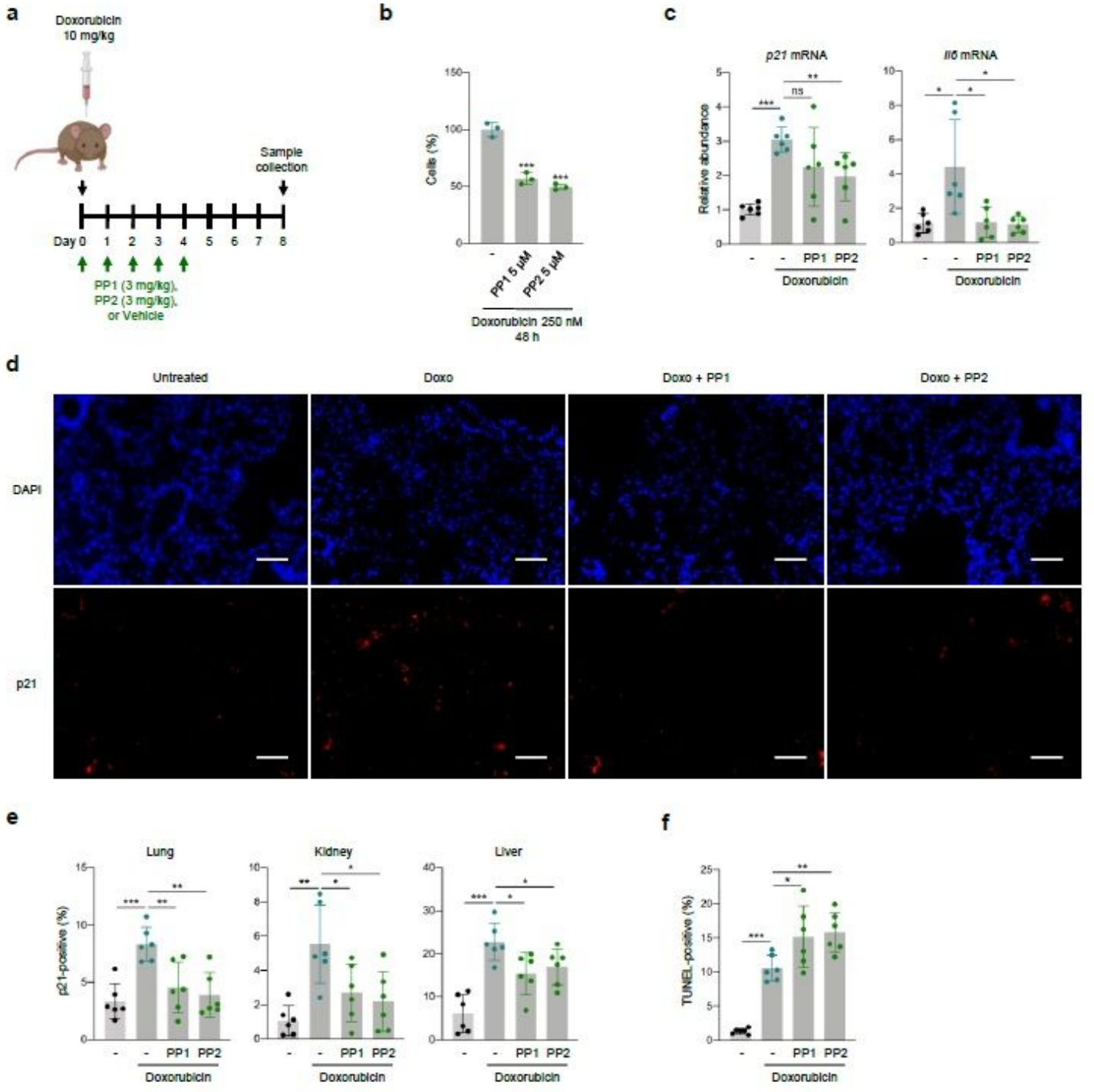


## Figure 7

SRC inhibition prevents accumulation of senescent cells in chemotherapy-induced senescence in mice. a Overview of the schedule of experiments performed in mice. b Viability of IMR-90 fibroblasts treated with senescence-inducing doxorubicin doses (250 nM) plus either vehicle, PP1, or PP2, as measured by direct cell counting 48 hours later. c Measurement of the levels of p21 and Il6 mRNAs by RT-qPCR analysis in lungs treated as in (a); data were normalized to Actb mRNA levels. d Representative micrographs of p21 immunofluorescent staining of the experimental groups indicated. Scale bar, 50 μm. e Quantification of

p21-positive cells in each tissue assayed. See also Supplementary Fig. 7c,d. f Percentages of TUNEL-positive cells in lungs from the indicated experimental groups. See also Supplementary Fig. 7e. Graph in b shows the mean values ± SD of n=3 independent experiments. Graphs in c, e, and f display the means (bars) and each individual value as a dot ± SD of n=6 mice; significance (*, $P < 0.05$, **, $P < 0.01$, ***, $P < 0.001$) was determined by using two-tailed Student's t-test.

## Supplementary Files

This is a list of supplementary files associated with this preprint. Click to download.

- AnerillasetalSupplementaryTextandFiguresfinal.pdf
- Supplementaltable1.pdf
- SupplementaryTable2.pdf